

THE GLOBAL EVOLUTION OF GIANT MOLECULAR CLOUDS I: MODEL FORMULATION AND QUASI-EQUILIBRIUM BEHAVIOR

MARK R. KRUMHOLZ*

Department of Astrophysical Sciences, Princeton University, Princeton, NJ 08544-1001

CHRISTOPHER D. MATZNER

Department of Astronomy, University of Toronto, Toronto, ON M5S 3H8

CHRISTOPHER F. MCKEE

Departments of Physics and Astronomy, University of California, Berkeley, Berkeley, CA 94720-7304

Accepted to the Astrophysical Journal, August 10, 2006

ABSTRACT

We present semi-analytic dynamical models for giant molecular clouds evolving under the influence of HII regions launched by newborn star clusters. In contrast to previous work, we neither assume that clouds are in virial or energetic equilibrium, nor do we ignore the effects of star formation feedback. The clouds, which we treat as spherical, can expand and contract homologously. Photoionization drives mass ejection; the recoil of cloud material both stirs turbulent motions and leads to an effective confining pressure. The balance between these effects and the decay of turbulent motions through isothermal shocks determines clouds' dynamical and energetic evolution. We find that for realistic values of the rates of turbulent dissipation, photoevaporation, and energy injection by HII regions, the massive clouds where most molecular gas in the Galaxy resides live for a few crossing times, in good agreement with recent observational estimates that large clouds in local group galaxies survive roughly 20 – 30 Myr. During this time clouds remain close to equilibrium, with virial parameters of 1 – 3 and column densities near 10^{22} H atoms cm^{-2} , also in agreement with observed cloud properties. Over their lives they convert 5 – 10% of their mass into stars, after which point most clouds are destroyed when a large HII region unbinds them. In contrast, small clouds like those found in the solar neighborhood only survive ~ 1 crossing time before being destroyed.

Subject headings: H II regions — ISM: clouds — stars: formation

1. INTRODUCTION

Giant molecular clouds (GMCs) are the primary reservoirs of molecular gas within spiral galaxies. Star formation is tightly correlated with the molecular column density within spiral galaxies (Wong & Blitz 2002), and is therefore controlled by the formation and evolution of these giant clouds. In this and a subsequent paper we develop the theory of GMC dynamics and present semi-analytical models for GMC evolution. We rely on simplifying assumptions about the structure of the cloud and the properties of the surrounding interstellar medium in order to focus on clouds' global energy budget and dynamical state.

Observations show that stars form much more slowly than the free-fall rate in GMCs (Zuckerman & Evans 1974; Rownd & Young 1999; Wong & Blitz 2002; Gao & Solomon 2004; Wu et al. 2005), and any successful GMC model must explain why this should be. It is now widely held that collapse is inhibited primarily by intensely supersonic motions (Vázquez-Semadeni et al. 2003; Mac Low & Klessen 2004), rather than magnetic fields (Mouschovias & Spitzer 1976; Shu et al. 1987; McKee 1989). (Star formation is strongly suppressed in low-extinction regions of molecular clouds, beyond

what one would expect if the star formation rate were simply following the column density to some power, suggesting that magnetic fields may play a secondary role – Onishi et al. 1998, 1999, 2002; Johnstone et al. 2004 – though see Hatchell et al. 2005 who find that low column densities reduce but do not completely prevent star formation.) Simulations and analytic theory indicate that the observed level of turbulence in GMCs is sufficient to produce the observed rate of star formation (Krumholz & McKee 2005).

However, undriven supersonic turbulence decays via radiation from isothermal shocks with an e -folding time of roughly one cloud crossing time (Mac Low et al. 1998; Stone et al. 1998; Mac Low 1999; Padoan & Nordlund 1999), so undriven turbulence alone is not sufficient to prevent global collapse. Instead, GMCs must either be destroyed before their turbulent motions decay, or the turbulence must be continually driven. The mode of destruction is intimately related to the clouds' dynamical state. Unless a cloud is destroyed all at once, any internal agent of destruction is also an internal source for turbulent energy – and one strong enough to balance turbulent decay (Matzner 2002). Destruction from within therefore favors models that achieve energetic and dynamical equilibrium (e.g. McKee 1989), if only briefly. The alternative – that clouds are disrupted entirely by outside agents (e.g. Bonnell et al. 2006) – requires most of the cloud mass to remain gravitationally unbound, as

*Hubble Fellow

Electronic address: krumholz@astro.princeton.edu

Electronic address: matzner@cita.utoronto.ca

Electronic address: cmckee@astron.berkeley.edu

bound regions rapidly collapse to higher density and become impervious to external forces. This is very difficult to reconcile with observational estimates of GMCs lifetimes and ratios of kinetic to potential energy. We critique the hypothesis of unbound clouds in greater detail in § 7.

In the following sections, we investigate the properties of molecular clouds both stirred and destroyed by HII regions within the cloud volume. The models we present here are improved in several ways relative to prior work:

- Rather than enforcing strict mechanical or energetic equilibrium, we solve for the time evolution of a cloud's radius and turbulent velocity dispersion according to the time-dependent virial and energy equations. In an early discussion of this problem, McKee (1989) allowed for time dependence in the energy equation, but assumed virial equilibrium. Matzner (1999) and Matzner & McKee (1999) followed the evolution of GMCs using time dependent virial and energy equations, but neglected several terms in these equations that we model here. While our approach is still not a full numerical solution of the equations of gravity, radiation, and magnetohydrodynamics, this approach enables us to study cloud dynamics without ignoring the effects of feedback on GMC evolution, as most numerical simulations to date have done (e.g. Clark et al. 2005).
- We account self-consistently for the recoil of cloud matter from the sites of mass ejection. In addition to driving turbulence, inward recoil confines the cloud. Recoil confinement is equivalent to an additional (and variable) external pressure, which becomes dynamically significant when cloud destruction is rapid. Corresponding terms appear in the virial (§ 2.1, Appendix A) and energy (§2.2, Appendix B) equations.
- Our model for HII regions (§3.2) accounts for the scale-dependence of density and velocity structures within GMCs. Although this does not fully account for the three-dimensional structure of the turbulent cloud medium, it is a significant improvement over the uniform cloud model employed by Whitworth (1979), Williams & McKee (1997), and Matzner (2002).
- We apply the Krumholz & McKee (2005) prescription for the star formation rate within turbulent clouds. This formula accurately predicts the star formation rate on a variety of scales, from starburst galaxies to the dense precursors of individual star clusters (Tan et al. 2006; Krumholz & Tan 2006). We use it to govern the birth rate of ionizing associations (§ 4).
- Our dynamical simulations (§ 5) track the formation and evolution of many individual HII regions. This approach accounts for the finite lifetime of ionizing stars and the time delay associated with the deceleration of shells driven by HII regions, neither of which is negligible compared to GMC dynamical times.

We analyze the results of our models in § 6, discuss the implications of our findings in § 7, and summarize our conclusions in § 8. In a future work (Matzner, Krumholz, & McKee, 2006, in preparation, hereafter Paper II) we apply this model to the problem of GMC formation and evolution in the galactic environment, including the effects of spiral density waves.

We do make several approximations in our work (§ 7.4). We assume that the clouds are spherical and that they expand or contract homologously. We assume that the clouds are sufficiently massive that the energy injection is dominated by HII regions, not protostellar outflows, which based on the models of Matzner (2002) should be true for clouds of mass $\sim 10^5 M_\odot$ or more. Such clouds contain most of the molecular mass in the Galaxy. We neglect the possibility that the column density of the cloud must exceed a threshold in order for stars to form (e.g. McKee 1989). We neglect energy injection by HII regions after they reach pressure equilibrium with the surrounding medium. Finally, we neglect possible time dependent effects due to the ambient medium of the GMC: no mass can be added to the cloud, and the ambient pressure remains constant. Despite these approximations, the models we present in this Paper illustrate the degree to which GMC properties can be understood in terms of internal dynamics.

Obviously, real GMCs are not homogeneously expanding or contracting spheres with smooth density distributions, so the approximations we make to render the problem analytically tractable are quite limiting. For this reason one might be tempted give up on analytic treatment altogether and simply attempt to solve the problem numerically. Unfortunately, full numerical simulation of a giant molecular cloud, including the formation of multiple star clusters and the effects of their feedback, is not feasible with current codes and computers. Instead, one is forced to make numerous approximations regardless of whether one takes a numerical or analytic approach. Many numerical simulations of GMC evolution simply ignore feedback altogether (e.g. Clark et al. 2005), include it only from a single source and/or focus on size scales much smaller than an entire GMC (e.g. Dale et al. 2005; Li & Nakamura 2006), or focus on the galactic scale and lack the resolution to say anything about individual GMCs (e.g. Slyz et al. 2005; Tasker & Bryan 2006). For this reason, an analytic approach that allows us to include feedback provides a valuable complement to numerical results, and points out areas for future simulation in which new effects might be discovered by a more thorough treatment of the physics.

2. EVOLUTION EQUATIONS

We are interested in the global evolution and energy balance in GMCs, so we construct a simple model in which we neglect details of cloud structure. We consider a cloud with density profile $\rho = \rho_e (r/R_{cl})^{-k_\rho}$, where R_{cl} is the radius of the cloud edge, and ρ_e is the edge density. As we discuss below, we take $k_\rho = 1$ as typical of GMCs. We approximate that the cloud evolves homologously, so that k_ρ is constant. However, the cloud can expand or contract and can lose mass (via evaporation of gas by HII regions), so ρ_e and R_{cl} both vary in time. The cloud is embedded in an ambient medium of negligible density and constant pressure P_{amb} . We model evaporation of

gas from the cloud as a wind, into which cloud material is injected at a rate $\dot{\rho}$ (which we take to be negative). Gas that is injected into the wind travels radially outward with “kick” velocity \mathbf{v}'_{ej} relative to the radial velocity of the cloud at that radius. Homology requires that the mass loss rate follow the existing density profile, so

$$\dot{\rho} = \frac{\dot{M}_{\text{cl}}}{M_{\text{cl}}}\rho, \quad (1)$$

where M_{cl} is the total mass of the cloud. We assume that the wind is low density and escapes from the vicinity of the cloud quickly, so that we can neglect its gravitational interaction with the cloud. As we discuss in more detail in § 3.2, this is a reasonable model for mass evaporating from an HII region.

We neglect the possibility that turbulent motions within the cloud are likely to lead to a significant loss of mass. This seems justified, since in a GMC with a virial ratio of unity, roughly the value for observed GMCs, the 3D turbulent velocity dispersion is smaller than the escape speed from the GMC surface by a factor of ~ 2 . Since the distribution of velocities in a supersonically turbulent medium cuts off exponentially above the turbulent velocity dispersion (Krumholz et al. 2006a), there is a negligible amount of mass moving rapidly enough to escape. We also neglect the possibility that a GMC might gain mass during its evolution, due to continuing infall. This assertion is more problematic, and we discuss it in more detail in § 7.4.

Within the limitations of these assumptions, we derive the Eulerian Virial Theorem (EVT) and equation of energy conservation in Appendices A and B. We then use these to construct evolution equations for the the cloud.

2.1. Equation of Motion

We derive the equation of motion from the EVT for an evaporating homologously-moving cloud,

$$\begin{aligned} \frac{1}{2}\ddot{I}_{\text{cl}} = & 2(\mathcal{T} - \mathcal{T}_0) + \mathcal{B} + \mathcal{W} - \frac{1}{2}\frac{d}{dt}\int_{S_{\text{vir}}}(\rho\mathbf{v}r^2)\cdot d\mathbf{S} \\ & + 2a_{\text{I}}\dot{M}_{\text{cl}}R_{\text{cl}}\dot{R}_{\text{cl}} + \frac{1}{2}a_{\text{I}}\ddot{M}_{\text{cl}}R_{\text{cl}}^2 \\ & + \frac{3-k_{\rho}}{4-k_{\rho}}\dot{M}_{\text{cl}}R_{\text{cl}}v'_{\text{ej}}. \end{aligned} \quad (2)$$

The proof of this theorem is in Appendix A. In this equation I_{cl} is the cloud moment of inertia, \mathcal{T} is the total kinetic and thermal energy, \mathcal{T}_0 is the energy associated with the confining external pressure, \mathcal{B} and \mathcal{W} are the magnetic and gravitational potential energies, and the surface integral represents the rate of change of the flux of inertia across the surface S_{vir} that bounds the volume to which we apply the virial theorem. These are all terms that appear in the EVT for a cloud without a wind, and their formal definitions are given in the Appendix. The three additional terms represent the second derivative of cloud inertia caused by mass loss through the wind (the first two extra terms) and the rate at which recoil from the process of launching the wind injects momentum into the cloud (the final additional term).

We now evaluate each of these terms in the context of our model. The moment of inertia is $I_{\text{cl}} = a_{\text{I}}M_{\text{cl}}R_{\text{cl}}^2$, where $a_{\text{I}} \equiv (3 - k_{\rho})/(5 - k_{\rho})$, so its second derivative is

$$\frac{1}{2}\ddot{I}_{\text{cl}} = a_{\text{I}}M_{\text{cl}}\dot{R}_{\text{cl}}^2 + a_{\text{I}}M_{\text{cl}}R_{\text{cl}}\ddot{R}_{\text{cl}}$$

$$+ 2a_{\text{I}}\dot{M}_{\text{cl}}R_{\text{cl}}\dot{R}_{\text{cl}} + \frac{1}{2}a_{\text{I}}\ddot{M}_{\text{cl}}R_{\text{cl}}^2. \quad (3)$$

Next consider the kinetic term \mathcal{T} , which we evaluate by decomposing the velocity into large-scale homologous and fluctuating turbulent components (equation A8). This gives

$$\mathcal{T} = \frac{3}{2}M_{\text{cl}}c_{\text{cl}}^2 + \frac{1}{2}a_{\text{I}}M_{\text{cl}}\dot{R}_{\text{cl}}^2 + \mathcal{T}_{\text{turb}} + 2\pi P_{\text{amb}}(R_{\text{vir}}^3 - R_{\text{cl}}^3), \quad (4)$$

where c_{cl} is the sound speed in the cloud (assumed constant), $\mathcal{T}_{\text{turb}}$ is the term for turbulent motions, and the last term comes from the constant ambient pressure P_{amb} outside the cloud. We return to $\mathcal{T}_{\text{turb}}$ below. Note that our assumption of homologous motion implicitly neglects the possibility of significant rotational motions. Observed GMCs have negligible kinetic energies in overall rotation compared to turbulent motions or gravitational potential energy.

We use the same strategy for the gravitational and magnetic terms as for the kinetic term, dividing them into steady and fluctuating parts. The non-turbulent gravitational part is

$$\mathcal{W}_{\text{non-turb}} = -\frac{3}{5}a\frac{GM_{\text{cl}}^2}{R_{\text{cl}}}, \quad (5)$$

where

$$a = \frac{15 - 5k_{\rho}}{15 - 6k_{\rho}}. \quad (6)$$

In principle we should include a component of potential energy due to stars, but all observed molecular clouds have gas masses that greatly exceed their stellar masses. For this reason, we may neglect the stellar mass. For the non-turbulent magnetic component, we follow McKee et al. (1993). Let Φ be the total magnetic flux threading the cloud, so that the mean field within the cloud is $\bar{B} = \Phi/(\pi R_{\text{cl}}^2)$. From the the form of the magnetic energy term (equation A13), it is clear that the non-turbulent component of this term scales as $\mathcal{B}_{\text{non-turb}} \propto \bar{B}^2 R_{\text{cl}}^3$. We therefore define the constant b such that

$$\mathcal{B}_{\text{non-turb}} = \frac{b}{3}\bar{B}^2 R_{\text{cl}}^3 = \frac{b}{3\pi^2}\left(\frac{\Phi^2}{R_{\text{cl}}}\right). \quad (7)$$

The exact value of b depends on the topology of the magnetic field and on the background field B_0 , but it is generally of order unity, with $b = 0.3$ as a typical value (McKee et al. 1993). We now define the magnetic critical mass M_{Φ} by

$$M_{\Phi}^2 = \left(\frac{5b}{9\pi^2 a}\right)\frac{\Phi^2}{G}, \quad (8)$$

so that we have

$$\mathcal{B}_{\text{non-turb}} = \frac{3}{5}a\frac{GM_{\Phi}^2}{R_{\text{cl}}}. \quad (9)$$

We define the magnetic support parameter by

$$\eta_{\text{B}} = \frac{M_{\Phi}}{M_{\text{cl}}}. \quad (10)$$

With this definition, we can combine the non-turbulent magnetic and gravitational terms to find

$$\mathcal{W}_{\text{non-turb}} + \mathcal{B}_{\text{non-turb}} = -\frac{3}{5}a(1 - \eta_{\text{B}}^2)\frac{GM_{\text{cl}}^2}{R_{\text{cl}}}. \quad (11)$$

Now consider the turbulent components. First, we can neglect the turbulent component of the gravitational term because since most sub-regions of a molecular cloud are not self-gravitating (Krumholz & McKee 2005), and therefore have negligible potential energy in comparison to their kinetic or magnetic energies. We can therefore set $\mathcal{W} = \mathcal{W}_{\text{non-turb}}$. For the magnetic and kinetic turbulent components, McKee & Zweibel (1992) argue for equipartition of kinetic and magnetic energy. Stone et al. (1998) find in simulations of low plasma- β turbulence that magnetic energy is slightly sub-equipartition, $\mathcal{B}_{\text{turb}} \approx 0.6 \mathcal{T}_{\text{turb}}$, which McKee & Tan (2003) argue can be understood as the kinetic and magnetic energies reaching equipartition for motions transverse to the field, but not for motions along the field. We adopt the ratio of magnetic to kinetic energy found by Stone et al. (1998), so the combined turbulent kinetic and magnetic energies in the virial theorem are

$$2\mathcal{T}_{\text{turb}} + \mathcal{B}_{\text{turb}} \approx 2.6 \mathcal{T}_{\text{turb}} = 3.9 M_{\text{cl}} \sigma_{\text{cl}}^2, \quad (12)$$

where $\sigma_{\text{cl}} = \langle (v_z - v_{\text{cl},z})^2 \rangle_{\rho}^{1/2}$ is the one-dimensional mass-weighted turbulent velocity dispersion of the gas in the cloud.

Finally, we come to the surface terms, \mathcal{T}_0 and $(d/dt) \int_{S_{\text{vir}}} (\rho \mathbf{v} r^2) \cdot d\mathbf{S}$. We can make the latter term zero by choosing our virial surface to be well outside the cloud so that the density of cloud material on the surface is negligible. However, the pressure outside the cloud P_{amb} is non-zero, so

$$\mathcal{T}_0 = 2\pi P_{\text{amb}} R_{\text{vir}}^3. \quad (13)$$

Substituting into the EVT (2), we arrive at an equation of motion for the cloud:

$$a_{\text{I}} \ddot{R}_{\text{cl}} = 3.9 \frac{\sigma_{\text{cl}}^2}{R_{\text{cl}}} + 3 \frac{c_{\text{cl}}^2}{R_{\text{cl}}} - \frac{3}{5} (1 - \eta_{\text{B}}^2) a \frac{GM_{\text{cl}}}{R_{\text{cl}}^2} - 4\pi P_{\text{amb}} \frac{R_{\text{cl}}^2}{M_{\text{cl}}} + \left(\frac{3 - k_{\rho}}{4 - k_{\rho}} \right) \frac{\dot{M}_{\text{cl}}}{M_{\text{cl}}} v'_{\text{ej}}. \quad (14)$$

This equation is intuitively easy to understand. The left-hand side represents the acceleration of the cloud edge, which is equated with the force per unit mass due to internal turbulence and pressure (the first two terms), gravity and magnetic fields (the third term), external pressure (the fourth term), and recoil from the evaporating gas (the final term).

For convenience we wish to non-dimensionalize this equation. Let $M_{\text{cl}-0}$, $R_{\text{cl}-0}$, and $\sigma_{\text{cl}-0}$ be the initial mass, radius, and velocity dispersion of the cloud. We define the dimensionless variables $M = M_{\text{cl}}/M_{\text{cl}-0}$, $R = R_{\text{cl}}/R_{\text{cl}-0}$, $\sigma = \sigma_{\text{cl}}/\sigma_{\text{cl}-0}$, and $\tau = t/t_{\text{cr}-0}$, where $t_{\text{cr}-0} = R_{\text{cl}-0}/\sigma_{\text{cl}-0}$ is the crossing time of the initial cloud. In these variables (14) becomes

$$R'' = \frac{3.9 \sigma^2 + 3\mathcal{M}_0^{-2}}{a_{\text{I}} R} - \eta_G \frac{M}{R^2} - \eta_P \frac{R^2}{M} + \eta_R \frac{M'}{M} \quad (15)$$

where the primes indicate differentiation with respect to τ ,

$$\eta_G \equiv \frac{3a(1 - \eta_{\text{B}}^2)}{a_{\text{I}} \alpha_{\text{vir}-0}}, \quad (16)$$

$$\eta_P \equiv \frac{4\pi R_{\text{cl}-0}^3 P_{\text{amb}}}{a_{\text{I}} M_{\text{cl}-0} \sigma_{\text{cl}-0}^2}, \quad (17)$$

$$\eta_R \equiv \left(\frac{3 - k_{\rho}}{4 - k_{\rho}} \right) \frac{v'_{\text{ej}}}{a_{\text{I}} \sigma_{\text{cl}-0}} \quad (18)$$

and we have defined the initial Mach number

$$\mathcal{M}_0 \equiv \frac{\sigma_{\text{cl}-0}}{c_{\text{cl}}} \quad (19)$$

and non-thermal virial parameter (Bertoldi & McKee 1992)

$$\alpha_{\text{vir}-0} \equiv \frac{5\sigma_{\text{cl}-0}^2 R_{\text{cl}-0}}{GM_{\text{cl}-0}}. \quad (20)$$

If the cloud's initial state is in equilibrium and it is not losing mass, so $R'(0) = M'(0) = 0$, then the ambient pressure P_{amb} must be such that

$$\eta_P = \frac{3.9 + 3\mathcal{M}_0^{-2}}{a_{\text{I}}} - \eta_G. \quad (21)$$

Note that this will generally implies an ambient pressure higher than the mean in the ISM. We consider it realistic, however, because GMCs form in relatively overpressured regions, and because we have not included the weight of an atomic layer overlying the cloud. Once mass loss commences, there will be an additional recoil pressure.

2.2. Equation of Energy Evolution

To derive the evolution equation for the cloud energy, we begin with the general energy conservation equation for an evaporating homologous cloud, which we derive in Appendix B and for convenience repeat here:

$$\frac{d\mathcal{E}}{dt} = \frac{\dot{M}_{\text{cl}}}{M_{\text{cl}}} [\mathcal{E} + (1 - \eta_{\text{B}}^2)\mathcal{W}] - 4\pi P_{\text{amb}} R_{\text{cl}}^2 \dot{R}_{\text{cl}} + \left(\frac{3 - k_{\rho}}{4 - k_{\rho}} \right) \dot{M}_{\text{cl}} \dot{R}_{\text{cl}} v'_{\text{ej}} + \mathcal{G}_{\text{cl}} - \mathcal{L}_{\text{cl}}. \quad (22)$$

Here \mathcal{E} is the total cloud energy, and \mathcal{G}_{cl} and \mathcal{L}_{cl} are the rates of radiative energy gain and loss integrated over the entire cloud. This equation is easy to understand intuitively. The term $(\dot{M}_{\text{cl}}/M_{\text{cl}})\mathcal{E}$ is simply the mass loss rate times the energy per unit mass in the cloud. The term $(\dot{M}_{\text{cl}}/M_{\text{cl}})(1 - \eta_{\text{B}}^2)\mathcal{W}$ is the rate at which mass loss reduces the cloud energy via reduction of the gravitational and magnetic fields, both of which are proportional to the mass. The next two terms represent the rate at which the external pressure and the recoil force from launching the wind do work on the cloud. Finally, the last two terms are simply the rate of radiative gains and losses.

Using the same arguments as in § 2.1, we may write the total energy in the cloud as

$$\mathcal{E} = \frac{1}{2} a_{\text{I}} M_{\text{cl}} \dot{R}_{\text{cl}}^2 + 2.4 M_{\text{cl}} \sigma_{\text{cl}}^2 + \frac{3}{2} M_{\text{cl}} c_{\text{cl}}^2 - \frac{3}{5} a (1 - \eta_{\text{B}}^2) \frac{GM_{\text{cl}}^2}{R_{\text{cl}}}. \quad (23)$$

Note that the factor of 2.4 in the $M_{\text{cl}} \sigma_{\text{cl}}^2$ term comes from taking $\mathcal{T}_{\text{turb}} + \mathcal{B}_{\text{turb}} \approx 1.6 \mathcal{T}_{\text{turb}}$, and the 3/2 in front of the $M_{\text{cl}} c_{\text{cl}}^2$ term comes from the assumption that the ratio of specific heats for the cloud is $\gamma_{\text{cl}} = 5/3$. One might expect 7/5 instead, since the cloud is molecular and therefore diatomic. However, the lowest rotational or vibrational excitations of H_2 have excitation temperatures of several hundred K. Since the cloud is far colder than this, molecules never have enough energy to access their rotational and vibrational degrees of freedom, and the gas acts as if it were monatomic. The time derivative

of this is

$$\begin{aligned} \frac{d\mathcal{E}}{dt} = & \frac{1}{2}a_I\dot{M}_{\text{cl}}\dot{R}_{\text{cl}}^2 + a_I M_{\text{cl}}\dot{R}_{\text{cl}}\ddot{R}_{\text{cl}} + 2.4\dot{M}_{\text{cl}}\sigma_{\text{cl}}^2 \\ & + 4.8M_{\text{cl}}\sigma_{\text{cl}}\dot{\sigma}_{\text{cl}}\frac{3}{2}\dot{M}_{\text{cl}}c_{\text{cl}}^2 - \frac{6}{5}a(1-\eta_{\text{B}}^2)\frac{GM_{\text{cl}}\dot{M}_{\text{cl}}}{R_{\text{cl}}} \\ & + \frac{3}{5}a(1-\eta_{\text{B}}^2)\frac{GM_{\text{cl}}^2\dot{R}_{\text{cl}}}{R_{\text{cl}}^2}. \end{aligned} \quad (24)$$

Substituting \mathcal{E} and $d\mathcal{E}/dt$ into the energy equation (22), we find

$$\begin{aligned} a_I M_{\text{cl}}\dot{R}_{\text{cl}}\ddot{R}_{\text{cl}} + 4.8M_{\text{cl}}\sigma_{\text{cl}}\dot{\sigma}_{\text{cl}} \\ + \frac{3}{5}a(1-\eta_{\text{B}}^2)\frac{GM_{\text{cl}}^2}{R_{\text{cl}}^2}\dot{R}_{\text{cl}} = \\ -4\pi P_{\text{amb}}R_{\text{cl}}^2\dot{R}_{\text{cl}} + \left(\frac{3-k_{\rho}}{4-k_{\rho}}\right)\dot{M}_{\text{cl}}\dot{R}_{\text{cl}}v'_{\text{ej}} \\ + \mathcal{G}_{\text{cl}} - \mathcal{L}_{\text{cl}}. \end{aligned} \quad (25)$$

We may regard this as an evolution equation for σ_{cl} , which makes intuitive sense: the overall expansion and contraction of the cloud is dictated by the equation of motion, and the thermal energy per unit mass is fixed, so the turbulence acts as the energy reservoir, increasing or decreasing as the cloud gains or loses energy. Rearranging to solve for $\dot{\sigma}_{\text{cl}}$ and non-dimensionalizing as we have done with the equation of motion gives

$$\frac{4.8}{a_I}\sigma' = -\frac{R'R''}{\sigma} - \eta_G\frac{MR'}{R^2\sigma} - \eta_P\frac{R^2R'}{M\sigma} + \eta_R\frac{M'R'}{M\sigma} + \frac{\mathcal{G} - \mathcal{L}}{a_I M\sigma}, \quad (26)$$

where \mathcal{G} and \mathcal{L} are the dimensionless rates of radiative energy gain and loss, defined by

$$\mathcal{G} - \mathcal{L} = \left(\frac{R_{\text{cl}-0}}{M_{\text{cl}-0}\sigma_{\text{cl}-0}^3}\right)(\mathcal{G}_{\text{cl}} - \mathcal{L}_{\text{cl}}). \quad (27)$$

3. ENERGY SOURCES AND SINKS

In this section we evaluate the rates of radiative energy gain \mathcal{G} and loss \mathcal{L} , and the characteristic launch speed of evaporating gas v'_{ej} . Together with the equation of motion (15) and the energy equation (26), and the star formation rate (§ 4), this will completely specify the evolution of our model clouds.

3.1. Decay of Turbulence via Isothermal Shocks

GMCs are approximately isothermal because their radiative time scales are much shorter than their mechanical time scales. As a result, supersonic motions within the cloud generate radiative shocks that remove energy from the cloud. The problem of the decay of turbulent motions by supersonic isothermal shocks in both hydrodynamic and magnetohydrodynamic media has been studied extensively by numerical simulation (e.g. Mac Low et al. 1998; Stone et al. 1998; Mac Low 1999; Padoan & Nordlund 1999). Stone et al. (1998) finds that the dissipation time scale of the turbulent energy is $t_{\text{dis}} \equiv \dot{E}/E = 0.83\lambda_{\text{in}}/v_{\text{rms}} = 0.48\lambda_{\text{in}}/\sigma$, where λ_{in} is the length scale on which the energy is injected.

In reality, HII regions coming from associations of various sizes, winds, and gravitational contraction of the cloud will all contribute to turbulent motions and inject

energy on different length scales. However, we can estimate an effective length scale through a combination of observational and theoretical considerations. Observationally, turbulence in nearby GMCs appears to be driven on scales comparable to the cloud scale or larger (Basu & Murali 2001; Heyer & Brunt 2004), and theoretical estimates of the effective energy injection scale of HII regions suggest that this is also near the cloud scale (Matzner 2002). The longest wavelength mode that a cloud of radius R_{cl} can support is $\sim 4R_{\text{cl}}$, where the factor of four arises because the largest turbulent mode corresponds to overall expansion or contraction of the cloud, in which diametrically opposed points are moving in opposite directions. Motion in opposite directions corresponds to the points being half a wavelength apart, giving a total wavelength of twice the cloud diameter (Matzner 2002). Thus, we take the effective injection scale to be $\lambda_{\text{in}} = 4\phi_{\text{in}}R_{\text{cl}}$, where $\phi_{\text{in}} \leq 1$, and we take $\phi_{\text{in}} = 1$ as a fiducial value based on observations and theory. The (dimensionless) rate at which energy is radiated away due to decaying turbulence is

$$\mathcal{L} = \frac{\eta_{\text{v}}}{\phi_{\text{in}}} \frac{M\sigma^3}{R}, \quad (28)$$

where Stone et al.'s simulations give $\eta_{\text{v}} = 1.2$. Note that, in deriving this factor, we have used our result that the energy in the turbulence, including magnetic and kinetic contributions, is $2.4M_{\text{cl}}\sigma_{\text{cl}}^2$.

It is also worth noting the possibility that the measured energy loss rates are too high. Cho & Lazarian (2003) argue that Alfvén waves cascade and decay anisotropically, and that this anisotropy can reduce the decay rate. However, Cho & Lazarian argue that simulations to date have not captured this effect because they use an isotropic driving field that is unrealistic. Sugimoto et al. (2004) simulate filamentary molecular clouds, and find that Alfvén waves of certain polarizations decay more slowly than simulations have found. Even if neither of these effects apply, there are differences in the rate of decay in different simulations depending on how the turbulence is driven. The simulations of Mac Low (1999) give slightly lower dissipation rates, probably because in those simulations the turbulence is forced with a driving field that is constant in time, while in those of Stone et al. (1998) the driving field is determined randomly at each time step. While we feel that the Stone et al. approach is somewhat more realistic, this is by no means certain.

3.2. HII Regions

HII regions are the dominant source of energy injection into GMCs from within (Matzner 2002). We consider the effects of the HII region from a single association here, and extend our results to a population of associations to § 4.

3.2.1. Evolution of Individual HII Regions

We first describe the evolution of an HII region embedded in a molecular cloud, modifying the analysis by Matzner (2002) by allowing the mean ambient density and velocity dispersion to vary with radius r away from the formation site of an association, as $\rho(r) \propto r^{-k_{\rho}}$ and $\sigma(r) \propto r^{-k_{\sigma}}$, respectively. Matzner (2002) considered only the homogeneous case $k_{\rho} = k_{\sigma} = 0$. Note that the

local turbulent virial parameter $\alpha(r) \equiv 5r\sigma^2(r)/[GM(r)]$ scales as $r^{k_\rho - 2k_\sigma - 2}$. Since $\alpha(r)$ is roughly unity on the scale of the cloud and on that of the newborn association (else it would not have formed), it is reasonable to assume $k_\rho = 2k_\sigma + 2$. The observed line width-size relation and density-size relations (Solomon et al. 1987) imply $k_\sigma = -1/2$ and $k_\rho = 1$, and we adopt these values below. These parameters correspond to a cloud with a negligible internal pressure gradient. Note that it has been suggested that the observational result $k_\rho = 1$ (which is equivalent to GMCs having constant column densities within a galaxy) is simply an observational artifact (e.g. Vazquez-Semadeni et al. 1997). However, many of the proposed mechanisms to explain how this artifact could be created do not apply to extragalactic observations, and more recent observations show that GMCs in other galaxies also show constant column densities (Blitz et al. 2005, and references therein). We discuss this point in more detail in § 6.2 and § 7.3, and also refer readers to the discussion of this point in Krumholz & McKee (2005).

The density variation affects the expansion phase of the HII region, and the variation in velocity dispersion affects how HII regions merge with the background turbulence. The evolution of an HII region in a turbulent GMC is a substantial problem that must ultimately be solved via simulation. However, to date only preliminary attempts to solve the problem have been made (e.g. Dale et al. 2005; Mellema et al. 2005; Mac Low et al. 2006; Krumholz et al. 2006b), so we are forced to rely on analytic approximations.

First, consider the expansion phase of an HII region. Assume that it has expanded well beyond its initial Strömgen radius. The mean ambient density is $\bar{\rho}(r) \propto r^{-k_\rho}$ within a distance r from the association, the ionized gas temperature is $T_{\text{II}} \simeq 7000$ K, the (constant) ionizing luminosity is $S = 10^{49} S_{49} \text{ s}^{-1}$, and the recombination coefficient is $\alpha^{(2)}$ in the on-the-spot approximation. If the HII region is blister-type, ionized gas will rocket away from the ionization front at a velocity $v'_{\text{ej}} = 2c_{\text{II}}$, where $c_{\text{II}} = 9.74 \text{ km s}^{-1}$ is the sound speed in the ionized gas. This is the characteristic launch velocity of our cloud's escaping wind. For the evolution of the HII region, Matzner's dynamical equation [his eq. (15)] admits the self-similar solution

$$r_{\text{sh}}^2 \bar{\rho}(r_{\text{sh}}) = (2, 1) \times \frac{3(7 - 2k_\rho)^2}{4(9 - 2k_\rho)} \rho_{\text{II}} c_{\text{II}}^2 t^2 \quad (29)$$

for (blister, embedded) regions, respectively. Here r_{sh} is the radius of the shell at time t , and ρ_{II} is the (uniform) density inside the HII region, which must vary as $r_{\text{sh}}^{-3/2}$ to ensure that ionizations balance recombinations. This equation applies when the expansion velocity is much larger than the turbulent velocity dispersion; we discuss the effects of turbulence below. This yields

$$r_{\text{sh}}^{7/2} \bar{\rho}(r_{\text{sh}}) = (2, 1) \times 2.2 \frac{3(7 - 2k_\rho)^2}{2(9 - 2k_\rho)} k_B T_{\text{II}} \left(\frac{3S}{4\pi\alpha^{(2)}} \right)^{1/2} t^2 \quad (30)$$

where k_B is Boltzmann's constant. The leading factor of 2.2 accounts for the particle abundances assuming helium is singly ionized. We assume blister-style regions hereafter, because GMCs are porous and therefore even small HII regions are likely to be able to punch through to low

density channels and vent (Matzner 2002). For our fiducial case $k_\rho = 1$, the mean column $\Sigma \equiv 4\bar{\rho}(r)r/3$ is a constant. Adopting $\alpha^{(2)} = 3.46 \times 10^{-13} \text{ cm}^3 \text{ s}^{-1}$, and adjusting the effective ionizing luminosity downward by a factor 1.37 to account for dust absorption (Williams & McKee 1997), we find

$$r_{\text{sh}} = 15.4 S_{49}^{1/5} \left(\frac{t}{3.8 \text{ Myr}} \right)^{4/5} \left(\frac{0.03 \text{ g cm}^{-2}}{\Sigma} \right)^{2/5} \text{ pc.} \quad (31)$$

Here we have normalized Σ to a typical value for Milky Way molecular clouds. We take the typical ionizing lifetime to be 3.8 Myr because we adopt the Kroupa (2001) initial mass function (IMF) and the stellar ionizing luminosities and lifetimes tabulated by Parravano et al. (2003). However, the lifetime can fluctuate from this for small clusters, so we define t_{ms} as the main-sequence ionizing lifetime of stars in a given cluster. (With these choices, a young association large enough to fully sample the IMF emits 3.4×10^{46} ionizing photons per second per solar mass, and has one star above $8M_\odot$, hence one supernova, per 131 solar masses.) The momentum of the HII region during this driving phase is

$$p_{\text{sh}} = 5.1 \times 10^{43} S_{49}^{3/5} \left(\frac{t}{3.8 \text{ Myr}} \right)^{7/5} \times \left(\frac{0.03 \text{ g cm}^{-2}}{\Sigma} \right)^{1/5} \text{ g cm s}^{-1}. \quad (32)$$

Assuming the gas can escape freely, the mass evaporation rate from the cloud is simply

$$\dot{M}_{\text{cl}} = -\dot{p}_{\text{sh}}/(2c_{\text{II}}). \quad (33)$$

Note that equations (31) and (32) are quite insensitive to the actual escape of ionized gas (Matzner 2002), but \dot{M}_{cl} depends on the existence of an escape route.

After the driving stars burn out at $t = t_{\text{ms}}$ (and if it has not yet merged with the cloud turbulence, § 3.2.2), the HII region will continue to expand in a momentum-conserving snowplow, in which $\dot{r}_{\text{sh}} \propto r_{\text{sh}}^{-(3-k_\rho)} \rightarrow r_{\text{sh}}^{-2}$ so that

$$r_{\text{sh}} = [r_{\text{ms}}^3 + 3r_{\text{ms}}^2 \dot{r}_{\text{ms}}(t - t_{\text{ms}})]^{1/3}, \quad (34)$$

where r_{ms} and \dot{r}_{ms} are the radius and velocity of the expanding shell at the time when the driving stars burn out. No mass is evaporated in this phase; we ignore the possibility of dynamical mass ejection by the snowplow unless the snowplow contains enough kinetic energy to unbind the cloud as a whole.

We now comment on two potential criticisms of our HII regions. First, real molecular clouds are very inhomogeneous, being filled with clumpy and filamentary structure. To what degree should this affect the results of this section? Very little, we argue. McKee et al. (1984) consider HII regions in a medium composed entirely of dense clumps. Adopting a clump mass distribution very similar to that observed within molecular clouds, they find (their eq. 5) that the photoevaporative rocket effect clears all but a couple clumps from within $r_{\text{sh}}(t)$. Additional homogenization, not considered by McKee et al., should come from the ram pressure stripping of overdense clumps and filaments as they are struck by gas already set in motion. For these reasons we expect the gross

properties of HII regions to be rather insensitive to local inhomogeneities. Recent simulations by Mellema et al. (2005) and Mac Low et al. (2006) support this expectation, and Mellema et al. find that the radius of an HII region in a turbulent medium as a function of time is very similar to what one would find in a uniform medium. (The simulation by Dale et al. (2005) gives a somewhat different result, but its different initial conditions and brief duration do not allow a fair comparison. In particular, Dale et al. compare their HII region expansion rate to the analytic solution for a uniform medium, despite the fact that they are simulating a strongly centrally condensed gas cloud.) For these reasons we expect our results to be robust against clumping of the gas on scales smaller than $r_{\text{sh}}(t)$. Given that our adoption of blister-type flow reflects the existence of inhomogeneities on scales larger than $r_{\text{sh}}(t)$, we expect the results in this section to be robust against cloud inhomogeneities in general.

A second potential criticism concerns our assumption that each HII region expands as if the gas density drops off like r^{-k_ρ} away from it. Formally this can only be consistent with our approximations of a spherical, $\rho \propto r^{-k_\rho}$ cloud if every HII region is born at the cloud center. We consider this to be merely a technicality. While our global cloud model refers only to a mean density profile and a turbulent energy, our model for the local density enhancement reflects the fact that clusters are born at the peaks of the turbulent density profile – which will not always occur at the cloud center. Indeed, we model mass loss and recoil pressure as if HII regions peppered the entire cloud and commonly vent out its side, and we ignore the interaction between regions.

Although our local $k_\rho = 1$ density is an idealization, we consider it an improvement over previous works which assumed homogeneous cloud gas. Moreover, the most luminous HII regions, those which dominate the energy injection, are in reality likely to be born near cloud centers, and once they have expanded to a radius that is significantly larger than the distance from their center to the peak of the density distribution in the GMC, the approximation that they are expanding down a $k_\rho = 1$ density gradient will be quite good.

3.2.2. Merging of HII regions

The shell will continue to expand until it decelerates to the point where the expansion velocity is comparable to the current velocity dispersion in the GMC, at which point the shell will break up, merge with the general turbulent motions, and cease to be a coherent entity. The HII region experiences a velocity dispersion $\sigma(r) = \sigma(r/R_{\text{cl}})^{-k_\sigma}$ after expanding to radius r , and we approximate that the merger occurs when $\sigma(r_{\text{sh}}) = \dot{r}_{\text{sh}}$. If the cloud properties were to remain fixed during the expansion, the merger radius of an HII region would be

$$r_m = \left(\frac{2p_{\text{sh}}}{M_{\text{cl}}\sigma} \right)^{1/(3-k_\sigma-k_\rho) \rightarrow 2/5} R_{\text{cl}}, \quad (35)$$

applying $k_\rho \rightarrow 1$ and $k_\sigma \rightarrow -1/2$. The factor of 2 arises from our idealization of the cloud as a sphere and the HII region as a hemisphere. Equation (35) holds whether merging occurs in the driving phase ($p_{\text{sh}} \rightarrow p_{\text{sh}}(t)$) or the snowplow phase ($p_{\text{sh}} \rightarrow p_{\text{sh}}(t_{\text{ms}})$). However, since the

cloud velocity dispersion and radius can change during the expansion of an HII region, equation (35) holds only approximately.

Note that gravity has little effect on HII regions except during merging, because their shells travel faster than $\sigma(r)$ up to that point. Indeed, the crossing time $r/\sigma(r)$ is $2.0\alpha(r)^{-1/2}$ times the free-fall time on scale r . Since $\alpha(r) \geq 1$, gravity only marginally affects shell motions. For this reason, we are justified in continuing to use our similarity solution (which neglects gravity) up to the point at which a shell merges.

3.2.3. Energy injection

At any given time, the cloud energy terms \mathcal{T} and \mathcal{M} include both the turbulent energy from merged HII regions, and the kinetic energy of those that are still expanding. During its expansion, the kinetic energy of a single HII region is

$$\mathcal{T}_1 = \frac{1}{2}p_{\text{sh}}\dot{r}_{\text{sh}} + 2\pi P_{\text{II}}r_{\text{sh}}^3, \quad (36)$$

the two terms reflecting bulk and thermal energy, respectively, if P_{II} is the internal pressure. The bulk kinetic energy at the time of merging t_m is therefore $\mathcal{T}_1(t_m) = p_{\text{sh}}\sigma(r_m)/2$.

Consider first the energy injected into turbulence at merging. We assume a merging shell stores the same fraction of energy in non-kinetic form as does the background turbulence, so we consider the total energy contribution to be $1.6\mathcal{T}_1(t_m)$. Rather than track individual regions' contributions in detail, we lump them together in the energy budget in a way that reproduces the correct average energy in turbulence. Since the cloud's energy dissipation time is $t_{\text{dis}} = 2.0(1.2\phi_{\text{in}}/\eta_v)R_{\text{cl}}/\sigma_{\text{cl}}$, whereas the dissipation of a single contribution occurs over $t_{\text{dis},1} = 2.0(1.2\phi_{\text{in}}/\eta_v)r_m/\sigma(r_m)$, we add

$$\Delta E_{\text{turb},1} = \eta_E \frac{r_m \sigma_{\text{cl}}}{R_{\text{cl}} \sigma(r_m)} \times 1.6\mathcal{T}_1 \rightarrow \eta_E \left(\frac{r_m}{R_{\text{cl}}} \right)^{1/2} \times 1.6\mathcal{T}_1, \quad (37)$$

rather than $1.6\mathcal{T}_1$, to the turbulent energy. The factor η_E parameterizes our ignorance of the exact efficiency with which HII regions drive motions in molecular clouds. For a uniform medium $\eta_E = 1$, but there has been some suggestion that $\eta_E < 1$ in turbulent media (e.g. Elmegreen 2000; Dale et al. 2005), although other simulations do not appear support this result (e.g. Mellema et al. 2005). In our models we vary η_E to see explore how sensitively our results depend on the efficiency with which HII regions inject energy.

We exclude from consideration the energy that expanding shells possess prior to merging (which we estimate to be several times smaller than the mean turbulent energy contributed by these regions). We note that the cloud outside of a given region is unaffected by it, except gravitationally, until it has merged. Thus, the rate of energy injection due to a single HII region is roughly

$$\mathcal{G}_{\text{cl}} = 1.6\eta_E \mathcal{T}_1 \left(\frac{r_m}{R_{\text{cl}}} \right)^{1/2} \delta(t - t_m), \quad (38)$$

and when a shell merges with the overall cloud turbulence we set

$$\frac{3}{2}\sigma_{\text{new}}^2 = \frac{3}{2}\sigma_{\text{old}}^2 + \eta_E \frac{\mathcal{T}_1}{M_{\text{cl}}} \left(\frac{r_m}{R_{\text{cl}}} \right)^{1/2}. \quad (39)$$

3.2.4. Cometary HII regions and cloud disruption

Finally, note that it is possible that a shell will contain enough momentum to expand to the point where its radius is larger than the cloud radius. If the expansion velocity of the shell at this point is larger than the escape velocity of the cloud (i.e. $\dot{r}_{\text{sh}} > \sqrt{2GM_{\text{cl}}/R_{\text{cl}}}$), then the shell will simply unbind the cloud. This criterion for cloud disruption is somewhat different from those adopted by Williams & McKee (1997) and Matzner (2002); we discuss the distinction and its implications in § 6.1. If the expansion velocity is smaller than the escape velocity, the shell will deform the cloud into a cometary configuration (Bertoldi & McKee 1990), but what happens at that point depends on whether or not the shell is still being driven by an active association. An undriven shell will neither gain nor lose energy once $r_{\text{sh}} > R_{\text{cl}}$, and its energy will eventually be added to the cloud's as turbulence once the cloud falls back. We therefore approximate that any shell in the snowplow phase that reaches $r_{\text{sh}} > R_{\text{cl}}$ but does not have enough momentum to unbind the GMC merges with the turbulence. On the other hand, a shell with an active source can continue to gain energy and evaporate mass even after reaching the cometary configuration, although eventually its energy will saturate. Following Williams & McKee (1997), we estimate that a shell can continue gaining energy after reaching the cometary phase up to a time $t \sim 2t_R$, where t_R is the time it took the HII region to reach R_{cl} . Its radius at this time will be $r_{\text{sh}} = 1.74R_{\text{cl}}$. If a driven HII region reaches this radius and still does not have enough energy to unbind the cloud, then it can affect the cloud no further. We approximate that the HII region merges with the turbulence and evaporates no further mass after that point.

It is important to point out that our treatment of large HII regions, and our criteria for cloud disruption and deformation into a cometary configuration, are quite approximate. In comparison to Matzner (2002), the criteria we use here reduce the shell momentum required to disrupt a cloud by roughly a factor of 2. This may affect our conclusions about the frequency of disruption by HII regions.

3.3. Supernovae and Protostellar Outflows

Here we discuss in more detail two sources of feedback that we have chosen not to include: supernovae and protostellar outflows. We omit these because they deliver much less energy per unit mass of stars than HII regions. Here we summarize the arguments, many of which are given in Matzner (2002), as to why this is the case.

The dynamics of a supernovae exploding inside HII regions, and the amount of energy and momentum they add, may be studied directly either by numerical simulation (e.g. Tenorio-Tagle et al. 1985; Yorke et al. 1989) or analytic calculation (Matzner 2002). Both methods yield similar results: supernovae generally sweep up enough mass inside their ionized bubbles to become radiative by the time they reach the outer boundary of their host HII regions. As a result, supernova blast waves radiate away much of their energy before encountering any molecular cloud material, and consequently increase the total mass removed by their HII region by at most $\sim 20 - 40\%$, and more typically $\sim 10\%$. Moreover, this applies only to

supernova progenitors whose HII regions are enclosed by the cloud and do not blister. Supernovae inside blister-type regions will deposit most of their energy outside the cloud, into the low density ambient medium, and should therefore have an even smaller effect. The assumption sometimes made in the literature (e.g. Clark et al. 2005) that supernovae can halt star formation and disrupt molecular clouds in $\lesssim 10$ Myr does not appear to be supported by any numerical or analytic calculations.

Protostellar outflows are negligible compared to HII regions on the size scale of entire GMCs for two reasons. First, the momentum injected into a cloud by an outflow is of order $\dot{M}_* v_w$, where \dot{M}_* is the star formation rate and $v_w \sim 40 \text{ km s}^{-1}$ is the rough momentum input per unit mass of stars formed for hydromagnetic winds (Matzner & McKee 2000; Richer et al. 2000). In contrast, as the analysis of § 3.2 shows, the momentum carried by HII regions is of order $\dot{M}_{\text{phot}} c_{\text{II}}$, where \dot{M}_{phot} is the rate at which ionizing photons photoevaporate cloud mass. While v_w is larger than c_{II} by roughly a factor of 4, the low star formation efficiencies of GMCs imply that the rate at which ionizing photons evaporate gas must exceed the rate at which the gas transforms into stars by a factor of $\gtrsim 10$, so $\dot{M}_{\text{phot}} \gg \dot{M}_*$. Our results in § 6 confirm this conclusion. Thus, HII regions provide much more momentum than outflows.

Second, outflows generally inject energy on significantly smaller scales than HII regions. While there are some spectacular examples of HH objects parsecs in size, these appear to be exceptions. Quillen et al. (2005) find in NGC1333 that the typical size of protostellar outflow cavities is only $\sim 0.1 - 0.2 \text{ pc}$. This is a low-to intermediate-mass star forming region, and cavities are likely to be even smaller in the denser environments where most Galactic star formation takes place. This is much smaller than the sizes comparable to the cloud radius reached by large HII regions (Matzner 2002). Following the discussion in § 3.1, we expect the energy injected by these outflows to decay much more quickly than the large-scale motions created by HII regions, and therefore make an even smaller contribution that comparison of the momenta would suggest.

It is worth noting that both arguments show that HII regions dominate over outflows only apply if we are concerned with objects comparable in size to entire GMCs. For smaller objects like the gas clumps forming individual clusters, the time for a single HII region to expand may be comparable to the evolution time of the entire region, and much of the energy of the HII region may be deposited outside the clump. As a result, outflows may well dominate for these objects (e.g. Quillen et al. 2005; Li & Nakamura 2006).

4. STAR FORMATION AND HII REGION CREATION

To know how HII region feedback affects GMC evolution, we must know the star formation rate and the clustering properties of the stars formed. To estimate the former, we use the turbulence-regulated star formation model of Krumholz & McKee (2005). This model postulates that stars form in any sub-region of the cloud where the local gravitational potential energy exceeds the turbulent kinetic energy, and it gives good agreement with simulations, with the observed star formation rate in the

Milky Way (Luna et al. 2006), with the age spreads of rich star clusters (Tan et al. 2006), with the star formation rate in dense molecular clumps (Krumholz & Tan 2006), and with the the Kennicutt-Schmidt Law for star formation in galactic disks (Kennicutt 1998). In the Krumholz & McKee model, the star formation rate is

$$\dot{M}_* = \text{SFR}_{\text{ff}} \frac{M_{\text{cl}}}{t_{\text{ff}}}, \quad (40)$$

where

$$\text{SFR}_{\text{ff}} \approx 0.073 \alpha_{\text{vir}}^{-0.68} \mathcal{M}^{-0.32}, \quad (41)$$

$t_{\text{ff}} \equiv [3\pi/(32G\bar{\rho})]^{1/2}$ is the free-fall time at the mean density $\bar{\rho}$ of the cloud, and α_{vir} and \mathcal{M} are the virial parameter and 1D Mach number. Thus, given the mass, radius, velocity dispersion, and gas temperature in a GMC, the Krumholz & McKee model enables us to predict the instantaneous rate of star formation in that cloud.

HII regions will be driven by the combined ionizing luminosity of all the stars in an association, and the energy injection therefore depends on how the stars are clustered. Thus we must estimate the ionizing luminosity function of associations as well as the star formation rate. This distribution is unfortunately quite uncertain, because a small cloud cannot form arbitrarily large associations and thus the Galactic-average and individual-cloud luminosity functions are different. Let $dF_a(\mathcal{N}_*)/d\ln\mathcal{N}_*$ be the fraction of OB associations with \ln number of stars between $\ln\mathcal{N}_*$ and $\ln\mathcal{N}_* + d\ln\mathcal{N}_*$ in the entire Galaxy, and let $dF_{a,M_{\text{cl}}}(\mathcal{N}_*)/d\ln\mathcal{N}_*$ be the corresponding fraction within a cloud of mass M_{cl} . McKee & Williams (1997) show that observations of the Galactic population of HII regions are consistent with a Galactic distribution

$$\frac{dF_a}{d\ln\mathcal{N}_*} \propto \frac{1}{\mathcal{N}_*}. \quad (42)$$

It will be more convenient for us to work with the mass of an association rather than the number of stars. Since we are concerned with OB associations which give rise to HII regions, and these have enough stars to sample the IMF well ($\mathcal{N}_* > 100$, Zinnecker et al. 1993), we convert from number to mass simply by multiplying by the mean stellar mass. We use the Kroupa (2001) IMF, which gives $\langle m \rangle_{\text{IMF}} = 0.21 M_{\odot}$, where $\langle \rangle_{\text{IMF}}$ indicates an average over the IMF. Thus,

$$\frac{dF_a}{d\ln M_a} \propto \frac{1}{M_a} \quad (43)$$

is the Galactic distribution of association mass M_a .

To go from the Galactic-average distribution to the individual cloud distribution, we follow Williams & McKee (1997) and Matzner (2002). First, we require that (1) no association has a mass larger than ϵM_{cl} , where Williams & McKee (1997) estimate $\epsilon = 0.1$, (2) the distribution of association masses within individual GMCs, when integrated over the GMC population of the Galaxy, gives the Galactic distribution (43), and (3) the star formation rate per cloud scales with the cloud mass as $\dot{M}_* \propto M_{\text{cl}}^{\beta}$. Using an argument analogous to the derivation of equation (16) in Williams & McKee (1997) and equation (35) in Matzner (2002), we derive a distribution

$$\frac{dF_{a,M_{\text{cl}}}}{d\ln M_a} \propto \frac{H(\epsilon M_{\text{cl}} - M_a)}{1 - (\epsilon M_{\text{cl}}/M_a)^{\alpha-\beta}} \left(\frac{1}{M_a} \right). \quad (44)$$

Here $H(x) = (1, 0)$ for $(x > 0, x < 0)$ is the Heaviside step function, and the Galactic population of star-forming GMCs satisfies $d\mathcal{N}_{\text{cl}}/d\ln M_{\text{cl}} \propto M_{\text{cl}}^{-\alpha}$ with $\alpha \approx 0.6$ to an upper limit of $M_u = 6 \times 10^6 M_{\odot}$ (Williams & McKee 1997). Based on their star formation model, Krumholz & McKee (2005) suggest $\beta \approx 0.67$, and we adopt this value in our work. Note that $\beta < 1$ implies a higher rate of star formation per unit mass in smaller clouds, which occurs because in the Galaxy smaller clouds have higher densities and thus shorter free-fall times. Equation (44) is fairly simple to understand intuitively: small clouds cannot make arbitrarily large associations, hence the factor $H(\epsilon M_{\text{cl}} - M_a)$. If all clouds produced OB associations with the same mass distribution as the Galactic powerlaw distribution, up to the maximum mass they could produce, there would be a deficit of large associations because all clouds can make small associations, but only a small fraction of clouds can make large ones. To offset this effect and produce the Galactic distribution of OB association masses, GMCs must be slightly more likely to produce an association near their upper mass limit than a straightforward extrapolation of the Galactic association mass distribution would suggest, hence the factor $[1 - (\epsilon M_{\text{cl}}/M_a)^{\alpha-\beta}]^{-1}$.

For large associations, the ionizing luminosity is simply

$$S_{49} = \frac{\langle s_{49}(m) \rangle_{\text{IMF}}}{\langle m \rangle_{\text{IMF}}} M_a, \quad (45)$$

and the main sequence ionizing lifetime is

$$\langle t_{\text{ms}} \rangle_a = \frac{\langle s_{49}(m) t_{\text{ms}}(m) \rangle_{\text{IMF}}}{\langle s_{49}(m) \rangle_{\text{IMF}}}, \quad (46)$$

where $s_{49}(m)$ and $t_{\text{ms}}(m)$ are the ionizing luminosity (in units of 10^{49} photons s^{-1}) and main-sequence lifetime of a star of mass m . We adopt the fits of Parravano et al. (2003) for $s(m)$ and $t_{\text{ms}}(m)$, which, together with the Kroupa (2001) IMF, give $\langle s_{49}(m) \rangle_{\text{IMF}} = 7.2 \times 10^{-4}$, $S_{49} = 3.4 \times 10^{-3} (M_a/M_{\odot})$, and $t_{\text{ms}} = 3.8$ Myr. However, for smaller associations the ionizing luminosity is likely to be dominated by the single most massive star, and this causes the ionizing luminosity function to flatten and the ionizing lifetime to vary with s_{49} . McKee & Williams (1997, Appendix A) give an analytic formula that approximates the flattening, but for semi-analytic models we can dispense with the approximation and determine the luminosity function simply by drawing stars randomly from the IMF until we accumulate mass up to a given association mass. We can then determine the ionizing luminosity of the association by summing those of the individual stars, and define the main sequence lifetime as the time at which the stars providing half the ionizing photons disappear.

Note that, in contrast to Williams & McKee (1997) and Matzner (2002), we do not impose an absolute upper limit of $S_{49} \leq 490$ on the ionizing luminosity of associations. This has no effect at all on any but the most massive clouds, since the requirement that the association mass be at most 10% of the cloud mass imposes a limit on S_{49} that is lower than this. For the most massive clouds we model in § 6.1, the largest associations formed reach $S_{49} \sim 1700$, but the extremely weak dependence of HII region properties on S_{49} ($r_{\text{sh}} \propto S_{49}^{1/5}$) means that increasing the maximum S_{49} by a factor of a few has very

little effect. Furthermore, due to the relative improbability of forming an association so close to the upper mass limit, even for our highest mass models the majority of clouds do not form associations with $S_{49} > 490$. Thus, we do not expect the presence or absence of an upper limit on association ionizing luminosities to affect our results in any significant way.

5. SEMI-ANALYTIC MODELS

5.1. Methodology

We now have in place all the necessary theoretical apparatus to set up our semi-analytic models. In essence, our model describes the evolution of a GMC using a pair of coupled non-linear ODEs, with added damping and driving terms. We integrate these equations forward in time in a three-step process. First, we use the current configuration of the cloud to compute the rate of turbulent decay (equation 28), the rate of star formation (equation 40), and the rate of evaporation by HII regions (equation 33). We update R_{cl} , \dot{R}_{cl} , σ_{cl} , and M_{cl} using these values (equations 15 and 26). We chose our update time step so that no quantity changes by more than 0.1% per advance. Second, we update the state of HII regions as described in § 3.2. We compute new values of the radius and expansion rate for each HII region, removing those whose expansion rates are low enough or radii are large enough for them to merge. At merging, we add their energy to turbulent motions in the cloud.

Third, we create new HII regions. To do this we generate a random mass for the next association, chosen from the distribution (44). We track the amount of mass transformed into stars since the last association was fully formed, and when half the next association mass has been accumulated in new stars, we add an HII region for that association. To determine the properties of the HII region, we generate stellar masses from the Kroupa (2001) IMF, assign an ionizing luminosity and main sequence lifetime to each star, and use these to compute the total ionizing luminosity and lifetime (defined as the time when the stars responsible for half the ionizing photons burn out) for the association. We continue to put newly formed stars into the new association until the full mass of the association has been accumulated, at which point we re-set the tally of accumulated stellar mass and randomly generate a new mass for the next association.

We terminate the evolution when one of three conditions has been satisfied: (1) an HII region unbinds the cloud (i.e. $r_{\text{sh}} \geq R$ and $\dot{r}_{\text{sh}} > \sqrt{2GM/R}$); (2) the cloud surface density has dropped to the point where its visual extinction $A_V < 1.4$, the minimum required for CO to remain molecular (van Dishoeck & Black 1988), assuming the standard Milky Way interstellar UV field and dust to gas ratio, whereby 1 g cm^{-2} corresponds to $A_V = 214$; or (3) the time step is less than 10^{-8} times the current evolution time, which occurs if the radius is approaching zero. We term these possibilities *disruption*, *dissociation*, and *collapse*. An important caveat that applies to all these outcomes is their dependence on our assumption of spherical symmetry. Even if an HII region delivers an impulse capable of unbinding a cloud, the cloud may actually be displaced as a whole, or it may break into multiple pieces, each of which is internally bound and capable of continuing to form stars. In the case of dis-

TABLE 1
FIDUCIAL PARAMETERS.

Parameter	Value
$\alpha_{\text{vir}-0}$	1.1
c_s	0.19 km s^{-1}
η_B	0.5
η_E	1.0
η_V	1.2
k_ρ	1.0
ϕ_{in}	1.0

sociation, a GMC's mean column density may be so low that much of its mass is turned atomic by the interstellar UV field, but overdense clumps within it may survive and continue star formation. Finally, the collapse case would probably result in a cloud fragmenting into smaller pieces rather than undergoing monolithic collapse as occurs in our one-dimensional models.

5.2. Fiducial Initial Conditions

Here we describe a basic set of initial conditions for our runs. In § 6, we discuss how varying some of these affects the outcome of our runs. Our models start with a common set of initial parameters summarized in Table 1. Most of these values are taken directly from observations, but a few of the parameters deserve some additional discussion. Observations of the strength of magnetic fields in GMCs are quite uncertain. We set $\eta_B = 0.5$, corresponding to equipartition between magnetic and kinetic energy. For a more detailed analysis of the observational data and theoretical arguments for this choice, see Krumholz & McKee (2005, § 7.3). We set $\eta_V = 1.2$ and $\phi_{\text{in}} = 1.0$, corresponding to the decay of turbulence at the rate found by the simulations of Stone et al. (1998), and to turbulence on the size scale of the entire GMC. Finally, we set $\eta_E = 1$, corresponding to HII regions injecting energy into turbulent media as efficiently as they would for smooth media.

With these parameters fixed, we can fully specify the initial conditions for a model by giving the initial mass and column density of a cloud. We evolve models with masses of $M_{\text{cl},6} = 0.2, 1.0$ and 5.0 , where $M_{\text{cl}} = M_{\text{cl},6} \times 10^6 M_\odot$. These masses span the range where most of the molecular gas in the Milky Way resides (Williams & McKee 1997). We set the initial cloud column density to $N_{H,22} = 1.5$, where $N_H = N_{H,22} \times 10^{22} \text{ cm}^{-2}$, which is typical for Milky Way GMCs regardless of mass (Larson 1981; Solomon et al. 1987). We summarize the initial radius, velocity dispersion, and crossing time as a function of mass in Table 2. For reference, we also show how these quantities vary with column density at fixed mass.

6. RESULTS

6.1. Fiducial Runs

We simulate the fiducial initial conditions 100 times each, using different random seeds for each run, for each of our three initial masses. Table 3 summarizes the statistical outcome of our fiducial runs.

The most basic result is that massive clouds attain a quasi-equilibrium state, in which the decay of turbulence is roughly balanced by the injection of energy by HII

TABLE 2
INITIAL CLOUD PROPERTIES.

$M_{\text{cl},6}$	$N_{\text{H},22}$	$R_{\text{cl}-0}$ (pc)	$\sigma_{\text{cl}-0}$ (km s $^{-1}$)	$t_{\text{cr}-0}$ (Myr)
0.2	0.5	33.7	2.37	13.9
1.0	0.5	75.3	3.54	20.8
5.0	0.5	168	5.30	31.1
0.2	1.5	19.4	3.12	6.1
1.0	1.5	43.5	4.66	9.1
5.0	1.5	97.2	6.97	13.6
0.2	4.5	11.2	4.10	2.7
1.0	4.5	25.1	6.14	4.0
5.0	4.5	56.1	9.18	6.0

regions. In this state, cloud virial parameters fluctuate around unity, but most clouds spend most of their lives with virial parameters from 1 to 3, with a time-averaged value from 1.5 – 2.2 depending on the cloud mass, as shown by Figure 1. This may slightly overestimate the true virial parameter, because in our model we assume that all of the energy from HII regions goes into random turbulent motions that can then fuel cloud expansion, rather than into coherent motions of the cloud as a whole or, if HII regions fragment the cloud, into motions of these fragments. Such coherent motions are often excluded in observational estimates of virial parameters. Nonetheless, at a qualitative level the result that clouds equilibrate to virial parameters ~ 1 is in good agreement with observations showing that massive clouds are approximately virialized (Heyer et al. 2001; Blitz et al. 2005).

The evolution follows a sawtooth pattern, in which an HII region drives up the virial parameter, which then exponentially decays until it is increased by the next injection of energy. This is similar to the pattern seen in simulations by Li & Nakamura (2006), in which turbulence in star-forming clumps ~ 1 pc in size is maintained by energy injection from protostellar outflows. This equilibrium is maintained partly because the star formation rate responds to the current state of the cloud, increasing as the cloud contracts and its turbulence decays, and going back down when the cloud re-expands. Figure 2 shows the depletion time, defined as the ratio of the current cloud mass to the current star formation rate, which exhibits this pattern.

As shown in Figure 3, cloud column densities also show a sawtooth pattern, oscillating up and down but remaining relatively constant over multiple expansion and contraction cycles so that the time average is roughly the observed value $N_{\text{H},22} \approx 1.5$. (The figure is somewhat deceptive, because the longest lived-clouds tend to go to somewhat lower column densities, and these stand out the most when examining the figure because the shorter-lived clouds all overlie one another on the left side of the plot. The numerically-computed time-averaged density over all models is given in Table 3.) Over their lifetimes, the average star formation efficiency of clouds, defined as the fraction of initial cloud mass transformed into stars, is 5 – 10%. HII regions ionize away anywhere from 50 – 90% of the mass before finally destroying the clouds entirely, with lower mass clouds losing less mass to photoionization than more massive clouds. Figure 4 shows this evolution.

The duration and stability of cloud equilibrium is af-

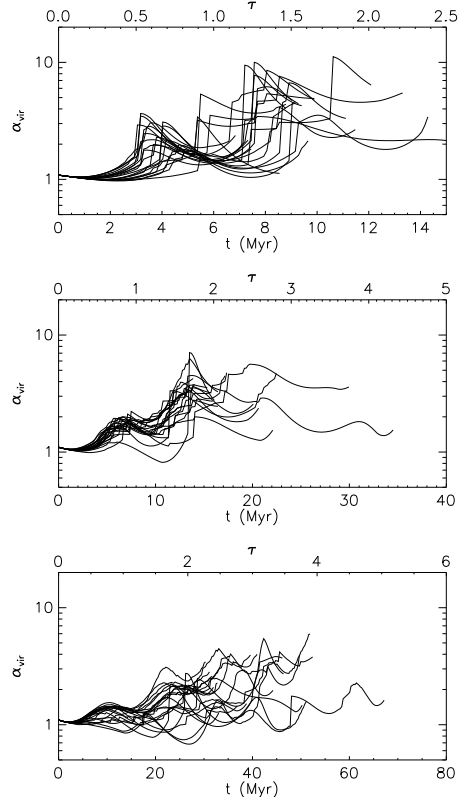


FIG. 1.— Virial parameter α_{vir} versus physical time t and dimensionless time τ for a sample of runs with fiducial parameters. We show $M_{\text{cl},6} = 0.2$ (top panel), $M_{\text{cl},6} = 1.0$ (center panel), and $M_{\text{cl},6} = 5.0$ (bottom panel).

ected by cloud mass. Low mass clouds, $M_{\text{cl},6} = 0.2$ are only stable for an average of 1.6 crossing times (3.2 free-fall times), and are most often destroyed when they form an HII region that delivers enough momentum to completely unbind them. They survive only one or a few cycles of expansion and contraction. In contrast, very massive clouds, $M_{\text{cl},6} = 5$, are stable for 3.2 crossing times and for multiple cycles before finally being unbound by HII regions. At all masses most clouds are destroyed by direct disruption rather than by a photodissociation, with the number photodissociated dropping sharply as a function of mass. This result is largely a function of cloud lifetimes. Direct disruption by a single HII region occurs when a truly large association forms, one that is on the tail of the mass distribution. Since larger clouds live longer and form more stars, they sample this tail more thoroughly, and thus are more likely to form one very large association capable of disrupting them than smaller clouds. An additional effect comes from the cloud velocity dispersion. Since larger clouds have higher velocity dispersions, the HII region shells driven by small associations merge more quickly, so the relative amount of energy injected by large versus small associations increases.

Cloud disruption is much more frequent in our models than in those of Williams & McKee (1997) or of Matzner (2002). The primary difference is a revised criterion for dynamical disruption. Williams & McKee took the onset of a cometary phase to be the point at which an HII region effectively disrupts or displaces its parent cloud.

TABLE 3
FIDUCIAL RUN OUTCOMES.

$M_{\text{cl},6}$	t_{life} (Myr)	$\bar{\alpha}_{\text{vir}}$	$\bar{N}_{H,22}$	SFE	M_{phot}	N_{disrupt}	N_{dissoc}	N_{col}
0.2	1.6 (9.9)	2.2	1.4	0.053	0.59	63	37	0
1.0	2.2 (20)	2.1	1.3	0.054	0.70	92	8	0
5.0	3.2 (43)	1.5	1.5	0.082	0.80	99	1	0

NOTE. — Col. (2): Mean lifetime in crossing times (Myr). Cols. (3-4): α_{vir} and $N_{H,22}$ averaged over all times and runs. Col. (5): Star formation efficiency. Col. (6): Fraction of mass photoevaporated prior to cloud destruction. Cols. (7-9): Number of runs out of 100 that ended in disruption, dissociation, and collapse.

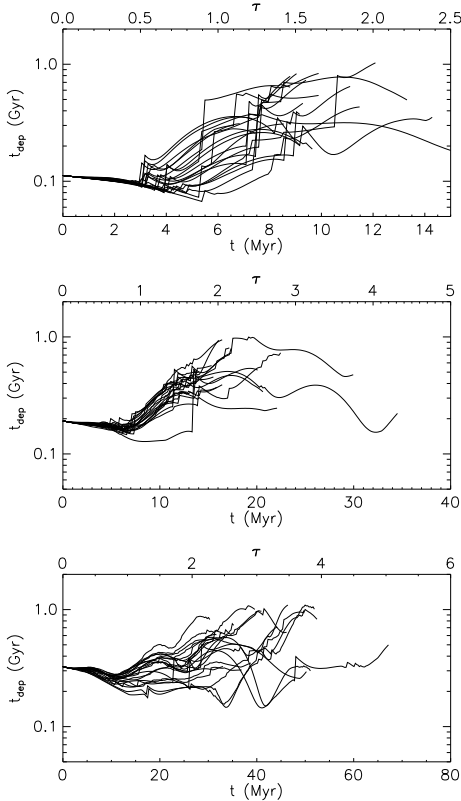


FIG. 2.— Depletion time versus physical time t and dimensionless time τ for a sample of runs with fiducial parameters. We show $M_{\text{cl},6} = 0.2$ (top panel), $M_{\text{cl},6} = 1.0$ (center panel), and $M_{\text{cl},6} = 5.0$ (bottom panel).

Matzner considered the delivery of a momentum p_{sh} in excess of $M_{\text{cl}}v_{\text{esc}}$ to define disruption. Our criterion ($\dot{r}_{\text{sh}} > v_{\text{esc}}$ when $r > R_{\text{cl}}$) resembles the Matzner threshold, but requires roughly half as much momentum because we model HII regions as hemispheres and clouds as spheres. In addition, our adoption of the Kroupa (2002) IMF and Parravano et al. (2003) stellar properties leads to about twice as many ionizing photons per stellar mass relative to Williams & McKee and Matzner. The revised model of HII region expansion also plays a minor role. All told, the largest cloud that can be disrupted by HII regions is about ten times more massive in this work than in the Matzner models. Our disruption criterion, being more generous than the Williams & McKee or Matzner criteria, accounts in an approximate manner for cloud displacement and fragmentation by large HII regions.

Our conclusion that more massive GMCs survive

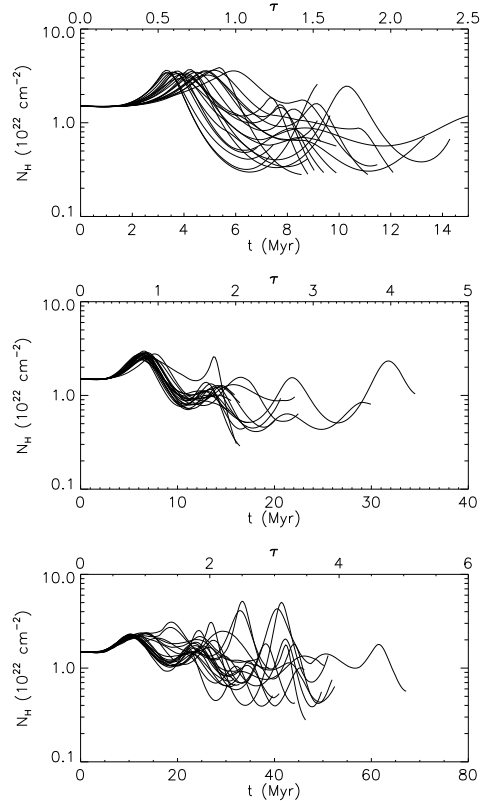


FIG. 3.— Column density N_H versus physical time t and dimensionless time τ for a sample of runs with fiducial parameters. We show $M_{\text{cl},6} = 0.2$ (top panel), $M_{\text{cl},6} = 1.0$ (center panel), and $M_{\text{cl},6} = 5.0$ (bottom panel).

longer than less massive ones also contrasts with the results obtained Williams & McKee (1997) and Matzner (2002). One reason for our different result is that in our model the star formation rate per unit mass is proportional to the inverse of the free-fall time, which, at constant N_H , produces more star formation per unit mass in small clouds than in large ones. Thus, low mass clouds are subject to more vigorous feedback. In contrast, previous studies generally adopted star formation laws under which the star formation rate per unit mass was independent of or increased with GMC size. This higher star formation rate compensates for the lack of large associations in small clouds and the ease with which small clouds can be driven into a cometary configuration, both of which tend to reduce mass loss. As a result clouds photoevaporate about the same fraction of their mass per dynamical time regardless of their starting mass.

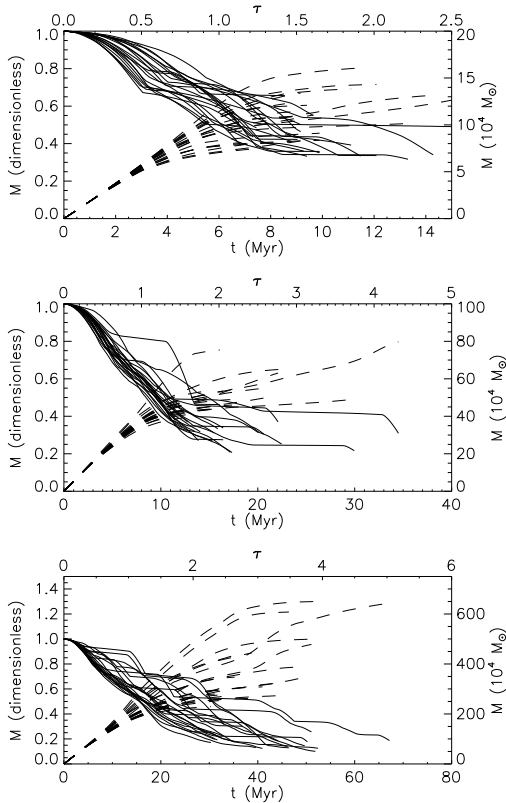


FIG. 4.— Cloud mass (*solid lines*) and 10 times mass of stars formed (*dashed lines*) versus physical time t and dimensionless time τ for a sample of runs with fiducial parameters. We show $M_{\text{cl},6} = 0.2$ (*top panel*), $M_{\text{cl},6} = 1.0$ (*center panel*), and $M_{\text{cl},6} = 5.0$ (*bottom panel*).

A second reason for our finding that small clouds live less time is our focus on the dynamical rather than the photoevaporation lifetime. For massive clouds, our models show that the photoevaporation e -folding time is $\sim 20 - 30$ Myr, comparable to or a bit shorter than the dynamical lifetime, and consistent with earlier estimates. In contrast, for low mass clouds the dynamical destruction time is shorter than the photoevaporation time. Clouds are dynamically broken up by HII regions, either by direct disruption from a single region or expansion to the point of photodissociation through the collective action of several HII regions, before most of their mass is photoevaporated away. This occurs because smaller clouds have less inertia and lower escape velocities, so they are more easily pushed apart by HII regions. Larger clouds require truly large HII regions to unbind them, and so are not disrupted until they have lost significant mass and enough associations have formed to reach to this tail of the distribution. Smaller clouds can be destroyed by more typical HII regions.

This distinction between photoevaporation and dynamical lifetime points to an important caveat of our analysis. The dynamical lifetime we find is the time for which a cloud exists as a single coherent entity under the assumption of spherical symmetry. As we discuss above, it is possible that, rather than unbinding all the molecular gas, or expanding it to the point of photodissociation, HII regions displace GMCs or blow GMCs into multiple pieces that are not bound to each other, but

each of which remains molecular and internally bound, and can continue forming stars. Thus, the time for which the Lagrangian elements of a cloud remain molecular and star-forming may be longer than the dynamical lifetime of the cloud which we have found. The photoevaporation time may provide a better estimate of this Lagrangian lifetime. For clouds of mass $M_{\text{cl},6} \gtrsim 1$ this distinction is not that significant since the lifetime is comparable to the photoevaporation time, but it can be for smaller clouds. Determining whether parts of these clouds do continue forming stars even after they no longer form a single gravitationally bound entity will require radiation hydrodynamic simulations that can include both cloud dynamics and photoevaporation.

6.2. Varying Column Density

Prompted in part by the result that giant molecular clouds both in the Milky Way (Larson 1981; Solomon et al. 1987) and in nearby galaxies with similar metallicities (Blitz et al. 2005) have a surprisingly small range of column densities, we investigate how varying the initial column density affects the evolution. For each mass we run with the fiducial parameters, we re-run using the same 100 random seeds but initial column densities of $N_{\text{H},22} = 0.5$ and 4.5 . The low column density case corresponds to a GMC with a mean column density that is just barely sufficient to be self-shielding against the interstellar UV field. Giant clouds of such low column density (as opposed to isolated low-mass clouds) have not been seen in CO surveys either in the Milky Way or in other local group galaxies, and there is observational evidence and theoretical expectation that molecular gas at column densities lower than $N_{\text{H},22} \sim 0.9$ is not star-forming (McKee 1989; Li et al. 1997; Onishi et al. 1998, 1999, 2002; Johnstone et al. 2004 – though see Hatchell et al. 2005, who find less star formation at low column densities, but not a complete absence of star formation). However, in the model of GMCs as turbulent density fluctuations, low column density clouds of all masses are expected to exist and be star-forming (e.g. Vazquez-Semadeni et al. 1997), so we consider the low column density case without imposing a column density threshold for star formation. The high column density case corresponds to GMCs found in galaxies that are entering the starburst regime. For example, in M64, a weak nuclear starburst galaxy, the typical GMC column density is 2.5 times that in the Milky Way (Rosolowsky & Blitz 2005).

Table 4 gives statistical results for the runs with varying N_{H} , and Figure 5 shows the evolution of column density versus time for a sample of runs at each mass. The results show that $N_{\text{H},22} \approx 1$ seems to be roughly a critical point in column density. Clouds that begin their evolution at substantially lower column density tend to disrupt or dissociate in ~ 1 dynamical time. Clouds that start at higher column densities show a pattern that depends on mass. At masses $M_{\text{cl},6} \ll 1$, they remain stable for long times. At higher masses, they tend to undergo uncontrolled collapse.

This change in behavior is not due to a change in the star formation rate per dynamical time. This is almost independent of the column density, since $\text{SFR}_{\text{ff}} \propto \mathcal{M}^{-0.32} \propto N_{\text{H}}^{-0.08}$ for fixed α_{vir} . Instead, the evolution depends on the column density because column density

TABLE 4
OUTCOMES WITH VARYING COLUMN DENSITY.

$M_{\text{cl},6}$	$N_{\text{H},22}$	t_{life} (Myr)	$\bar{\alpha}_{\text{vir}}$	$\bar{N}_{\text{H},22}$	SFE	M_{phot}	N_{disrupt}	N_{dissoc}	N_{col}
0.2	0.5	0.44 (6.1)	1.7	0.60	0.022	0.34	74	26	0
0.2	1.5	1.6 (9.9)	2.2	1.4	0.053	0.53	63	37	0
0.2	4.5	5.6 (15)	1.5	5.2	0.19	0.80	93	0	7
1.0	0.5	0.72 (15)	1.9	0.61	0.026	0.51	8	92	0
1.0	1.5	2.2 (20)	2.1	1.3	0.054	0.70	92	8	0
1.0	4.5	-	-	-	-	-	17	0	83
5.0	0.5	1.3 (41)	1.6	0.5	0.039	0.58	5	95	0
5.0	1.5	3.2 (43)	1.5	1.5	0.082	0.80	99	1	0
5.0	4.5	-	-	-	-	-	0	0	100

NOTE. — Column definitions are identical to those in Table 3, and cases with $N_{\text{H},22} = 1.5$ are identical to the values in that Table. We compute average quantities excluding runs that result in collapse, and we do not attempt to compute averages in cases where a majority of runs produce collapse.

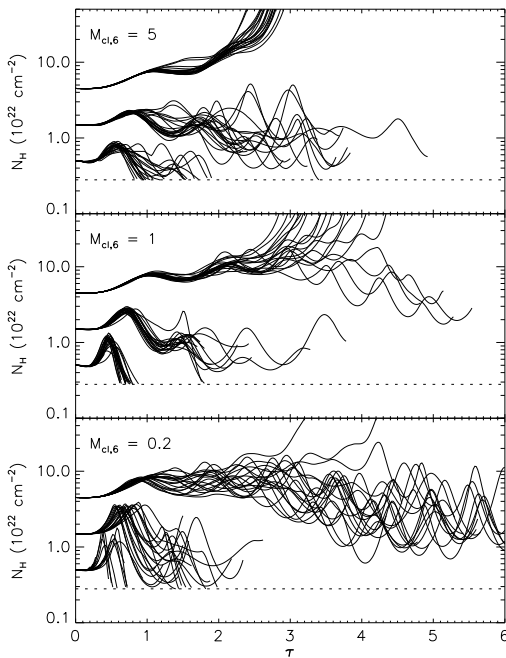


FIG. 5.— Column density N_{H} versus dimensionless time τ for a sample of runs with varying initial N_{H} . Each panel shows a different initial mass, shown in the upper left corner. The dotted horizontal line indicates the column density at which clouds dissociate.

significantly affects the efficiency of feedback. With our approximation that merged HII regions do not inject energy into clouds, the fraction of an HII region’s energy that is lost to radiation increases with column density, so for equal ionizing fluxes and times, the kinetic energy in an HII region shell varies as $N_{\text{H}}^{-3/5}$. Furthermore, higher column densities increase the cloud velocity dispersion (as $N_{\text{H}}^{1/4}$ for fixed α_{vir}) and decrease the expansion velocity, causing HII regions to break up and merge earlier. Since in our model HII regions only gain energy as long as they are expanding, the sooner they merge the less energy they inject. From equation (35), for fixed cloud and HII region properties the ratio of the merger radius to the cloud radius scales as $N_{\text{H}}^{-9/50}$. Combining these two effects, equation (38) shows that the energy injected by a single HII region of fixed properties into a cloud of fixed mass varies with column density as $N_{\text{H}}^{-69/100}$. Thus, the

efficiency with which ionizing photons are converted into turbulent motions is a reasonably strong function of the column density, and this picks out a particular characteristic column density at which energy injection balances loss. This turns out to be roughly the observed column density $N_{\text{H},22} \approx 1.5$. At this point we should mention one significant cautionary note: we have not explored the effects of the external environment of GMCs, and in particular the ambient pressure, on the characteristic column density. We will consider this effect in Paper II.

It is easy to understand intuitively why the critical column density above which clouds tend to collapse for masses $M_{\text{cl},6} \gtrsim 1$ should be between $N_{\text{H},22} = 1.5$ and 4.5. In the high column density case, the velocity dispersion required to hold up a cloud is almost more than HII regions can provide. HII regions cannot effectively drive turbulence to velocity dispersions larger than the ionized gas sound speed $c_{\text{II}} = 9.7 \text{ km s}^{-1}$, and as indicated in Table 2, in the high mass, high column density case the level of turbulence required to maintain $\alpha_{\text{vir}} = 1.1$ is $\sigma_{\text{cl}-0} = 9.2 \text{ km s}^{-1}$. For the medium mass case it is $\sigma_{\text{cl}-0} = 7.0 \text{ km s}^{-1}$. Furthermore, if the cloud contracts some so that its velocity dispersion increases a bit beyond these values, then HII regions will break up and merge with the turbulence almost immediately and will therefore inject very little energy. Matzner (2002) previously discussed the inability of HII regions to maintain virial balance in systems where the required velocity dispersion exceeds c_{II} , and our models find the same result. We discuss the implications of this in more detail in § 7.3. Note, however, that this conclusion is partially dependent on our approximation that HII regions cease driving turbulence once they cease dynamically expanding and merge, which may not be entirely correct – see § 7.4.

The long lifetime and high star formation efficiency produced at low masses and high column density also suggests an interesting interpretation: this combination of parameters may correspond to the regime of formation of individual OB associations and open clusters, which is characterized by relatively high column densities (McKee & Tan 2003) and star formation efficiencies $\gtrsim 10\%$ (Lada & Lada 2003), and probably requires many crossing times to complete (Tan et al. 2006). Although the highest column density we have considered is still relatively modest by the standards of some cluster-forming clumps, which can reach $N_{\text{H},22}$ of several tens,

the general result that low masses and high column densities can produce long-lived bound objects is suggestive. This is particularly true in light of the recent evidence that rich clusters require $\gtrsim 5$ crossing times to assemble (Tan et al. 2006; Huff & Stahler 2006; Krumholz & Tan 2006), and must therefore be held up against collapse yet not be unbound by feedback for at least this long.

6.3. Varying Dissipation Rate

As we discuss in § 3.1, it is possible that the turbulent dissipation rate may vary from our fiducial estimate, either being substantially lower if simulations of turbulent decay have missed some important physics, or substantially higher if the characteristic scale of molecular cloud turbulence is smaller than the size of an entire GMC. The latter possibility is probably ruled out by observations showing that turbulence in molecular clouds is self-similar out to the size of the entire GMC (e.g. Ossenkopf & Mac Low 2002; Heyer & Brunt 2004), but we explore it nonetheless to better understand how the dissipation rate affects GMC evolution. We re-run our fiducial case $\eta_v = 1.2$, $\phi_{\text{in}} = 1.0$, corresponding to turbulence on the GMC scale and decay at the rate measured by Stone et al. (1998), with $\eta_v = 0.4$, $\phi_{\text{in}} = 1.0$, corresponding to turbulence on the GMC scale decaying somewhat more slowly than Stone et al. find, and with $\eta_v = 1.2$, $\phi_{\text{in}} = 0.33$, corresponding to turbulence driven on 1/3 of the GMC size scale decaying at the Stone et al. rate. Since the dissipation rate depends on the ratio η_v/ϕ_{in} , we are therefore considering energy dissipation rates that are a factor of 3 smaller and larger than the fiducial case. (From equations 15, 26, and 28, this factor of 3 larger or smaller dissipation rate should correspond roughly to a factor of 3 change in the acceleration of the cloud radius, since $\mathcal{L} \propto \eta_v \sigma^3$, $\sigma' \propto \mathcal{L}/\sigma^2$, and $R'' \propto \sigma^2$.)

Table 5 summarizes the statistical results of varying the dissipation rate, and Figure 6 shows the evolution of column density versus time as a function of the dissipation rate and cloud mass. The general result is that, with the exception of the high mass, fast dissipation case, the results do not greatly depend on the dissipation rate. As the turbulent dissipation rate increases, the lifetime and mean virial parameter decrease and the mean column density and the star formation efficiency increase, but none of these changes by more than $\sim 10\%$. That changing the dissipation rate by a factor of three in either direction induces a much smaller change in the cloud column density and virial parameter suggests that these values represent roughly an equilibrium configuration, and that this equilibrium is quite robust. As the dissipation rate changes by a factor of nine from the lowest to the highest values we try, clouds contract a bit more, form stars a bit more vigorously, and are destroyed by stellar feedback a bit sooner, but only modest changes are sufficient to offset the change in dissipation rate. Star formation self-regulates to produce GMCs with $N_{\text{H},22} \approx 1$ and $\alpha_{\text{vir}} \approx 1 - 2$, and the regulation is stiff in the sense that even an order of magnitude change in the dissipation rate does not alter it much. We discuss reasons for this in § 7.1.

There are two exceptions to this, where varying the dissipation rate does produce a qualitative change in the outcome. For clouds of high mass and high dissipation rate, we see a phenomenon similar to the high mass, high

column density case. For $M_{\text{cl},6} = 5$, the velocity dispersion starts at $\sigma_{\text{cl},0} = 7.0 \text{ km s}^{-1}$, but increases very rapidly as the cloud contracts due to decay of turbulence. By the time the first large HII regions have expanded to the point where they contain substantial kinetic energy, the cloud has contracted to the point where the velocity dispersion required to hold it up is comparable to or larger than $c_{\text{II}} = 9.7 \text{ km s}^{-1}$. As a result, HII regions cannot hold up the cloud, and it collapses.

The other exception occurs if we simultaneously increase the column density to $N_{\text{H},22} = 4.5$ and lower the dissipation rate by setting $\eta_v = 0.4$, $\phi_{\text{in}} = 1.0$. In this case, clouds have long lifetimes and high star formation efficiencies regardless of their mass, and their column densities gradually decrease with time. Qualitatively, this is the same behavior we see for the case $M_{\text{cl},6} = 0.2$, $N_{\text{H},22} = 4.5$, and the fiducial dissipation rate. Figure 7 shows the evolution of clouds within initial column densities of $N_{\text{H},22} = 4.5$ as a function of mass and dissipation rate. As the plot shows, reducing the dissipation rate changes the characteristic mass at which one goes into the high star formation efficiency, long-lived regime. The boundary between this regime of very long stability and the regime of stability for a few dynamical times appears to depend weakly on both the mass and the dissipation rate.

6.4. Varying Energy Injection Efficiency

As we discuss in § 3.2.3, we are not certain of the efficiency with which HII regions are able to drive motions in turbulent media. We therefore re-run our fiducial models with $\eta_E = 0.25$, thereby reducing the amount of energy injected by HII regions by a factor of 4. This allows us to examine how strongly our results depend on our assumed efficiency.

Table 6 summarizes our results, which show how small a difference the change in driving efficiency makes. With a factor of 4 less energy injection for an HII region of the same luminosity, the mean lifetime of the lower mass clouds we model increases by about 10% and that of the highest mass clouds decreases by the same fraction. Mean virial parameters decline by $\sim 10\%$, and mean column densities rise a similar amount. Both star formation efficiencies and fractions of the mass photoevaporated rise, but again by only $\sim 10\%$. The only quantity that changes significantly is the fraction of clouds destroyed by dissociation, which not surprisingly declines sharply. Thus, our results appear extremely insensitive to changes in the assumed energy injection efficiency of HII regions. Figure 8, which shows the evolution of column density versus time for a sample of our runs, confirms this impression. The runs with lower energy injection efficiency go to slightly higher column densities, but overall show no major difference in their evolution from the fiducial case. Again, the star formation process seems to be self-regulating, so that large changes in efficiencies, either of energy injection or of dissipation, produce only very small changes in the global statistics of cloud evolution. We discuss reasons for this in § 7.1.

7. DISCUSSION

7.1. The Relationship of Cloud Properties to Rates of Radiative Loss and Energy Injection

TABLE 5
OUTCOMES WITH VARYING DISSIPATION RATE.

$M_{\text{cl},6}$	η_v	ϕ_{in}	t_{life} (Myr)	$\bar{\alpha}_{\text{vir}}$	$\bar{N}_{H,22}$	SFE	M_{phot}	N_{disrupt}	N_{dissoc}	N_{col}
0.2	0.4	1.0	1.7 (10)	2.8	1.2	0.046	0.53	49	51	0
0.2	1.2	1.0	1.6 (9.9)	2.2	1.4	0.053	0.59	63	37	0
0.2	1.2	0.33	1.4 (8.4)	1.9	1.8	0.067	0.57	44	56	0
1.0	0.4	1.0	2.3 (21)	2.6	1.1	0.046	0.64	90	10	0
1.0	1.2	1.0	2.2 (20)	2.1	1.3	0.054	0.70	92	8	0
1.0	1.2	0.33	1.7 (16)	1.7	2.1	0.074	0.74	61	35	4
5.0	0.4	1.0	4.4 (60)	2.3	1.0	0.070	0.75	98	2	0
5.0	1.2	1.0	3.2 (43)	1.5	1.5	0.082	0.80	99	1	0
5.0	1.2	0.33	-	-	-	-	-	0	0	100

NOTE. — Column definitions are identical to those in Table 3, and cases with $\eta_v = 1.2$, $\phi_{\text{in}} = 1.0$ are identical to the values in that Table. As in Table 4, we compute average quantities excluding runs that result in collapse, and we do not attempt to compute averages in cases where a majority of runs produce collapse.

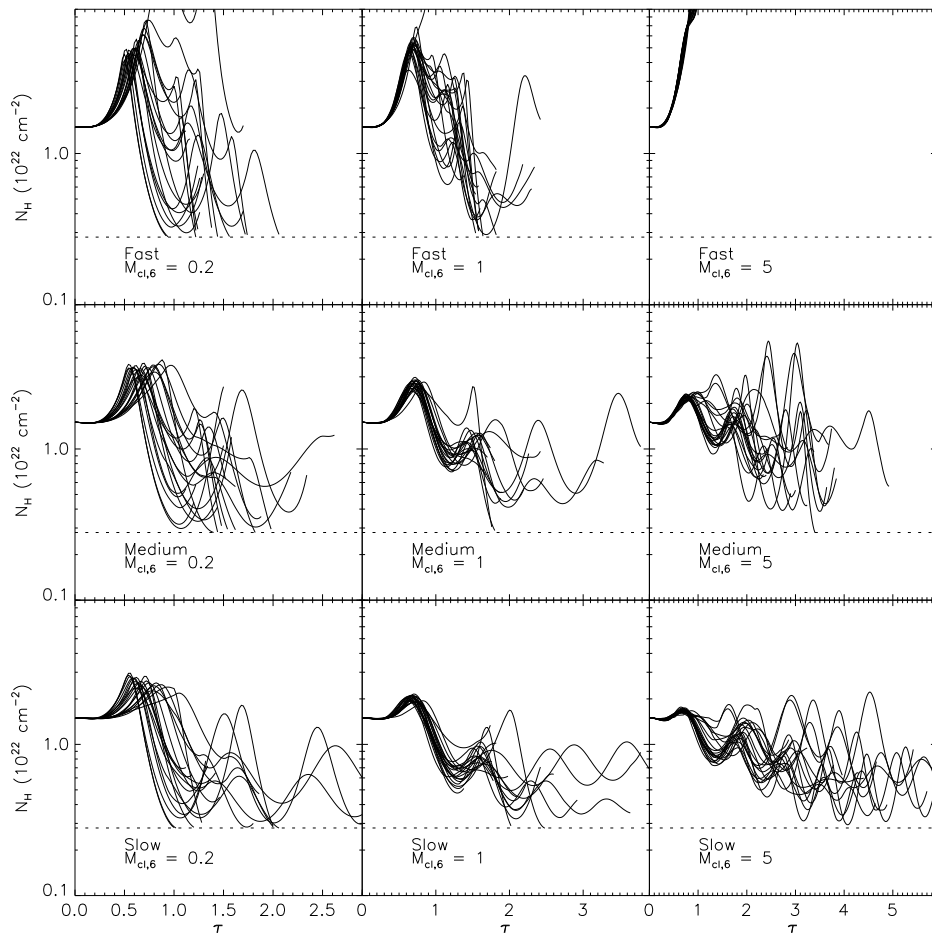


FIG. 6.— Column density N_H versus dimensionless time τ for a sample of runs with varying dissipation rates and masses. The mass and dissipation rate are indicated in each panel – slow is $\eta_v = 0.4$, $\phi_{\text{in}} = 1.0$, medium is $\eta_v = 1.2$, $\phi_{\text{in}} = 1.0$, and fast is $\eta_v = 1.2$, $\phi_{\text{in}} = 0.33$. The dotted horizontal line indicates the column density at which clouds dissociate. All runs begin with $N_{H,22} = 1.5$.

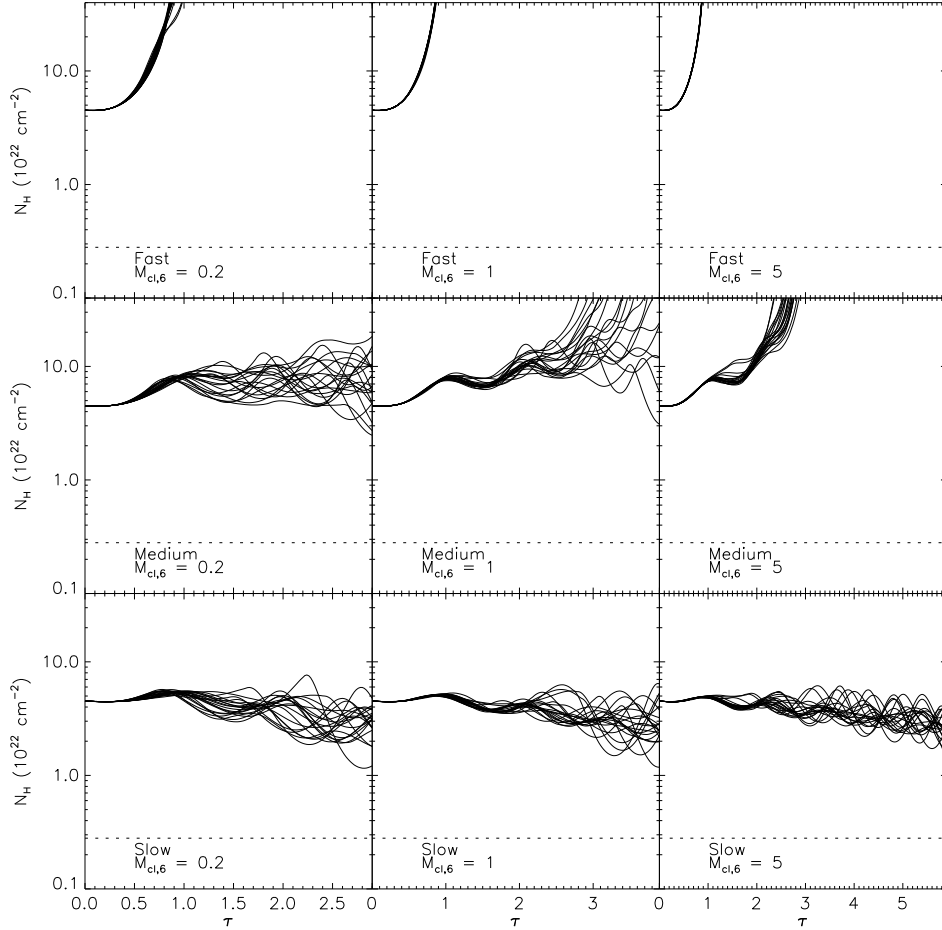


FIG. 7.— Column density N_H versus dimensionless time τ for a sample of runs with varying dissipation rates and masses, all starting from high initial column densities. The mass and dissipation rate are indicated in each panel – slow is $\eta_V = 0.4$, $\phi_{\text{in}} = 1.0$, medium is $\eta_V = 1.2$, $\phi_{\text{in}} = 1.0$, and fast is $\eta_V = 1.2$, $\phi_{\text{in}} = 0.33$. The dotted horizontal line indicates the column density at which clouds dissociate. All runs begin with $N_{H,22} = 4.5$.

TABLE 6
OUTCOMES WITH VARYING HII DRIVING EFFICIENCY.

$M_{\text{cl},6}$	η_E	t_{life} (Myr)	$\bar{\alpha}_{\text{vir}}$	$\bar{N}_{H,22}$	SFE	M_{phot}	N_{disrupt}	N_{dissoc}	N_{col}
0.2	0.25	1.7 (11)	1.6	1.7	0.065	0.67	93	7	0
0.2	1.0	1.6 (9.9)	2.2	1.4	0.053	0.59	63	37	0
1.0	0.25	2.1 (20)	1.6	1.6	0.062	0.75	100	0	0
1.0	1.0	2.2 (20)	2.1	1.3	0.054	0.70	92	8	0
5.0	0.25	2.8 (39)	1.3	1.8	0.087	0.82	100	0	0
5.0	1.0	3.2 (43)	1.5	1.5	0.082	0.80	99	1	0

NOTE. — Column definitions are identical to those in Table 3, and cases with $\eta_E = 1.0$ are identical to the values in that Table.

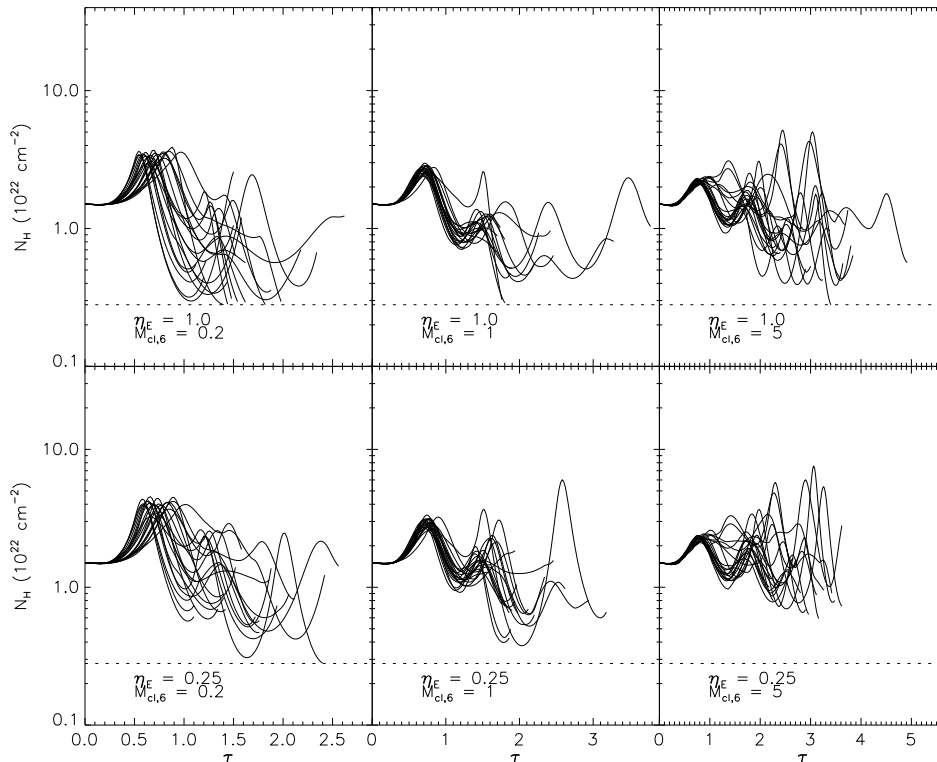


FIG. 8.— Column density N_H versus dimensionless time τ for a sample of runs with varying HII region driving efficiencies and masses. The mass and driving efficiency are indicated in each panel. The dotted horizontal line indicates the column density at which clouds dissociate. All runs begin with $N_{H,22} = 1.5$.

One of the most interesting results of our analysis is how little the global statistics of cloud evolution, such as lifetimes and star formation efficiencies, change in response to large changes in parameters such as the rate at which turbulence decays via isothermal shocks or the efficiency with which HII regions transfer their kinetic energy into turbulent motions. We can understand intuitively why large variations in either driving efficiency or dissipation rate cause such minimal changes in the statistics of cloud evolution by examining Figure 2. As the Figure illustrates, clouds form most of their stars during their contraction phases, when they reach high densities, so the rate of star formation is effectively set by the cadence of expansion and contraction cycles. This cadence is affected only slightly by the dissipation rate and the energy injection efficiency, because both of these properties are coupled to cloud evolution poorly, with large time delays.

For a GMC to contract from an expanded state, the rate-limiting step is not the time required to dissipate the energy injected by HII regions, it is the cloud free-fall time, the time the cloud would take to collapse even if it contained no turbulence at maximum expansion. Thus, varying the turbulent dissipation rate makes little difference to the cloud contraction time. Similarly, the time it takes for HII regions to drive apart a cloud is controlled less by the amount of energy added per unit mass of stars formed than by the time delay between when stars begin forming and when the HII regions they create expand, break up, and drive turbulent motions. Lowering the driving efficiency means that clouds expand somewhat less far, but since the dissipation rate of the turbulence is

a strong function of the velocity dispersion, $\mathcal{L} \propto \sigma^3$, the extra energy at early stages produced by higher efficiency is radiated away very quickly, and produces only slightly increased cloud expansion. We can put this argument more formally by noting that our energy equation gives $\sigma' \propto \sigma^2$, neglecting changes in velocity dispersion due to external pressure and cloud expansion, so the time required for a velocity dispersion of σ_0 immediately after a large HII region breaks up to decay to a value σ_1 obeys $t \propto (\sigma_0 - \sigma_1)/(\sigma_0\sigma_1)$. If the final velocity dispersion is much smaller than the initial one, i.e. $\sigma_1 \ll \sigma_0$, this ratio is independent of σ_0 . Thus, the decay time for a large amount of initial energy injected is only slightly larger than the decay time for a significantly smaller energy injection, so the cloud expansion time and maximum radius depend only weakly on the driving efficiency.

This insensitivity to the dissipation rate and the energy injection rate breaks down if the dissipation rate becomes so high or the energy injection so inefficient that HII regions are not capable of expanding clouds at all. In this case, clouds undergo runaway collapse. It also breaks down if the dissipation rate becomes so low or the efficiency so high that the first generation of HII regions simply unbinds most clouds, in which case clouds form only one generation of stars and are destroyed on a time scale set by the expansion time for HII regions from that first generation. However, in between these two extremes there is a broad range of parameter space within which the cadence of expansion and contraction cycles is set mostly by the cloud free-fall time and the time required for HII regions to break up, with only a very weak dependence on the details of the energy loss

rate or the energy gain efficiency. The degree of insensitivity is illustrated by Figures 6 and 8, in which factor of several variations in dissipation rate or driving efficiency change the expansion and contraction period by only tens of percent.

7.2. GMC Stability and Lifetime

Observations place strong constraints on the stability of giant molecular clouds, and are now beginning to constrain their lifetimes as well. We must test theories that seek to explain the behavior of GMCs against these observations. The first constraint is that giant molecular clouds cannot be in a state of global collapse. If they were, then they would convert order unity of their mass into stars in a crossing time, and this would produce a star formation rate two orders of magnitude larger than the observed one (Zuckerman & Evans 1974). Thus, a model of GMC evolution must explain why GMCs are stable against global collapse and convert only a few percent of their mass into stars per crossing time.

The second observational constraint is that GMCs, at least the most massive ones, live for considerably more than a single crossing time. While GMC lifetimes are quite difficult to estimate inside the Milky Way, age spreads of the largest OB associations are ~ 20 Myr (Blaauw 1964; Blitz & Shu 1980), which is a probable lower limit on the lifetimes of GMCs. More robust constraints are available in extragalactic observations, where there is no distance ambiguity. Associations between GMCs and star clusters imply a typical GMC lifetime of ~ 20 Myr in M33 (Engargiola et al. 2003) and 27 Myr in the LMC (Fukui et al. 1999; Blitz et al. 2005). This is significantly greater than the GMC crossing time of $\lesssim 10$ Myr. While the difference between one and a few crossing times might seem insignificant, recall that the e -folding time for the decay of turbulence is roughly a crossing time. A cloud two crossing times old will have lost almost all of its turbulence if feedback or some other source cannot replenish it, and will therefore undergo global collapse. Thus, the observations not only require that clouds be stable against collapse, they require that this stability be maintained for several turbulent decay times.

The GMC model we present in this Paper, using the fiducial parameters suggested by observation and previous theoretical work, provides very good qualitative agreement with the observations. We show that feedback from star formation can keep clouds supersonically turbulent and virialized for ~ 30 Myr, until they are destroyed by feedback. Combined with the results of Krumholz & McKee (2005) showing that supersonic turbulent motions naturally produce a star formation rate of a few percent per crossing time if star formation occurs in virialized clouds, this model satisfies both observational constraints. We discuss the question how GMCs evolve during this lifetime in more detail in § 7.3.

Alternative models run into difficulty with one of these two observations, or with other data. One possible explanation why GMCs do not undergo global collapse is that they are gravitationally unbound transient fluctuations in the atomic ISM; only local subregions constituting a small fraction of the cloud mass are bound and can collapse (Mac Low & Klessen 2004; Clark & Bonnell 2004; Clark et al. 2005; Vazquez-Semadeni et al. 2006;

Dobbs et al. 2006). However, in this case it is hard to see how GMCs could survive 20 – 30 Myr. For example, Clark et al. (2005) find GMC lifetimes of only about 10 Myr in their simulations of unbound clouds. There are also other severe observational difficulties. There are no molecular clouds with masses $\gtrsim 10^4 M_\odot$ that are clearly gravitationally unbound, with virial parameters $\alpha_{\text{vir}} \gg 1$, either in the Milky Way (Heyer & Brunt 2004) or in other galaxies (Engargiola et al. 2003; Rosolowsky et al. 2003; Rosolowsky & Blitz 2005; Blitz et al. 2005). There are many examples in the Milky Way of clouds of mass $< 10^4 M_\odot$ with virial parameters $\alpha_{\text{vir}} \gg 1$ (Heyer & Brunt 2004), and there is no obvious reason why massive clouds should not also display a range of α_{vir} if they are generally unbound. Transient fluctuation models also have problems explaining the existence of a GMC mass scale and the low rotation rates of GMCs. These arguments are presented in detail in Krumholz & McKee (2005).

A second possibility is that GMCs are bound, at least marginally, but that they are destroyed before the turbulence with which they are born decays away. As a result, they never have a chance to begin global collapse. However, the observed lifetimes of $\gtrsim 20$ Myr appear to rule out the possibility that such rapid destruction is the norm. Furthermore, to work this model requires a mechanism of cloud destruction that reliably operates in $\lesssim 1$ crossing time. As we show here, HII regions are not capable of completely photoevaporating or disrupting massive clouds over such short periods. Supernovae and protostellar winds inject considerably less energy into GMCs per unit mass of stars formed than do HII regions (Tenorio-Tagle et al. 1985; Yorke et al. 1989; Matzner 2002), so they are unlikely candidates for rapid cloud disruption. In the absence of a plausible mechanism for cloud disruption in ~ 10 Myr, this model faces a major theoretical problem as well as an observational one.

It is worth noting at this point that arguments for GMC lifetimes in the Milky Way strictly limited to 1 crossing time, e.g. Hartmann et al. (2001), generally rely on observations of clouds in the solar neighborhood, all of which are much smaller than the larger, more typical GMCs we have considered in this paper. Since we find that molecular clouds $\lesssim 10^5 M_\odot$ in mass do only survive for ~ 1 crossing time, our results are consistent with the idea that solar neighborhood GMCs are short-lived. We simply suggest that GMC lifetime is mass-dependent, and that the nearest clouds, due to their atypical masses, also have atypical lifetimes.

7.3. An Evolutionary Scenario for GMCs

Our findings allow us to present a rough evolutionary scenario for GMCs that is consistent both with the constraints of stability and GMC age described in § 7.2 and with the observation that GMCs in the Milky Way and in other galaxies all lie in a narrow range of column densities and virial parameters, centering around $N_{H,22} \approx 1.5$ and $\alpha_{\text{vir}} \approx 1 - 2$. (Larson 1981; Solomon et al. 1987; Blitz et al. 2005). This scenario is quite similar to that suggested in McKee (1989) and is developed in considerably greater detail in Paper II.

Our scenario is that GMCs are born at low column densities by condensation out of the atomic ISM, pri-

marily triggered by self-gravitational instabilities in spiral shocks (e.g. Kim & Ostriker 2001; Kim et al. 2002, 2003). This can only occur in regions of a galactic disk that are at significantly higher densities and pressures than is typical of the ISM. If star formation were able to start in such clouds immediately, they would undergo rapid disruption, converting $\lesssim 3\%$ of their mass into stars. However, in reality such clouds are probably not star-forming over most of their volume, so feedback is suppressed.

This may explain the observation that GMCs pass through a phase in which they appear to lack embedded HII regions. The duration of this phase is difficult to obtain from observations – Fukui et al. (1999), Engargiola et al. (2003) and Blitz et al. (2005) report that $\sim 1/4$ of GMCs do not show H α signatures associated with HII regions, but this is probably an overestimate because it does not include highly obscured HII regions. Although the H α sensitivities of the catalogs used by these authors are sufficient to detect HII regions with H α luminosities comparable to the Orion Nebula, Orion is visible largely because it is on the near side of a dark cloud; at the distance of the LMC or M33, Orion would be invisible if it were oriented with the dark cloud on the near side rather than the other way around. Spitzer/MIPS observations have failed to find any GMCs that are dark at $24\ \mu\text{m}$, so there must be some embedded star formation even in GMCs without detected HII regions (E. Rosolowsky, 2006, private communication). This result suggests either that the HII regions surveys are incomplete, or that clouds do not begin making massive stars until well after they have begun forming low mass stars, an effect we have not considered.

Regardless of how long this initial starless phase lasts, a question we will address using our models in Paper II, in the absence of feedback, GMCs will contract due to loss of turbulent support, gravity, and external pressure, until they approach $N_{H,22} \approx 1$. At that point, they become star-forming, and feedback stabilizes them against further contraction and keeps them in virial equilibrium for several crossing times. We observe GMCs at $N_{H,22} \approx 1$, $\alpha_{\text{vir}} \approx 1 - 2$ because this is where they spend the vast majority of their lifetimes. This column density is selected because it is the one for which energy injection by turbulence roughly balances energy loss by isothermal shocks. In addition to turbulent energy injection, the recoil momentum produced by mass being evaporated by HII regions may also play a significant role in confining clouds.

This quasi-equilibrium endures for an amount of time that depends on the cloud mass. For massive clouds, which contain most of the molecular mass in the Milky Way and in all but one other galaxy in which it is possible to estimate cloud mass distributions (Fukui et al. 1999; Engargiola et al. 2003; Blitz et al. 2005), it endures 2 – 3 crossing times, or 20 – 30 Myr. During a cloud’s lifetime, it converts 5 – 10% of its mass into stars. These results are robust against changes in the assumed dissipation rate for turbulence or efficiency of turbulent driving by HII regions. Less massive clouds are probably dynamically disrupted in ~ 1 crossing time, consistent with estimates of the lifetimes of small clouds in the solar neighborhood (e.g. Hartmann et al. 2001), although

parts of them may endure in molecular phase and continue forming stars for longer periods of time even after the original cloud has been disrupted.

One interesting question is how our results might change if we considered a galaxy quite different from the Milky Way. Observations indicate that GMCs in normal spiral galaxies like the Milky Way are generally quite similar to those in the Milky Way (Blitz et al. 2005), so to find truly different conditions we must consider galaxies that are approaching the regime of starbursts. The sole observational example of such a galaxy where we have observed the clouds is M64, a weak starburst in which the largest GMCs are $\gtrsim 10^7 M_{\odot}$ in mass, and have surface densities up to $N_H \approx 4 \times 10^{22}\ \text{cm}^{-2}$ (Rosolowsky & Blitz 2005). Despite these differences from Milky Way GMCs, observations indicate that these clouds are still in approximate virial balance, and that like Milky Way GMCs their star formation rate is only a few percent per free-fall time. Thus, they are not in a state of global collapse.

Since we have found that HII regions cannot sustain the turbulence and prevent collapse in such clouds (though see § 7.4), we are left with two possibilities. Either the dissipation rate in such clouds is lower than our fiducial estimate, or there is an additional source of energy input that supplements HII regions. One strong candidate for a source of energy injection is driving of turbulence by external shocks (Kornreich & Scalo 2000), either from supernovae, gravitational instabilities driven by the potential of the stars, or cloud-cloud collisions (Tan 2000). This mechanism encounters considerably difficulty in the Milky Way because GMCs are much denser than the gas around them in which shocks propagate. This creates an “impedance mismatch” that makes it difficult to drive turbulence into the GMCs (Nakamura et al. 2006). However, in a starburst where the ISM is entirely molecular, clouds are not much denser than their surroundings. Rosolowsky & Blitz (2005) find that in M64 the GMCs are overdense only by factors ~ 2 . This removes the impedance mismatch problem, and makes it far easier for external shocks to drive turbulence than it is in galaxies like Milky Way. Whether this mechanism can work in detail will require more analytic models and simulations to determine.

7.4. Limitations of This Model

The most obvious limitation of our model is the constraint that GMCs evolve homologously. In mathematical terms, this constraint is equivalent to dropping time derivatives of a_{I} in the virial theorem. This should only change our results substantially if changes in the moment of inertia of a GMC occurred primarily through changes in its shape rather than overall expansion or contraction. While a cloud in approximate equilibrium probably does experience most changes in its inertia via changes in shape, a cloud that is undergoing global collapse or global disruption would almost certainly experience most changes in its inertia through those processes rather than through changes in shape. As a result, our broad conclusion that neither overall collapse or disruption occur for several crossing times seems likely to be robust.

A more subtle limitation to our model is our simple boundary conditions for GMCs. For simplicity we have assumed a fixed mass budget and a fixed external pressure that puts GMCs into pressure balance initially. In

reality, GMCs may start forming stars while still accumulating gas. The somewhat higher mean mass for GMCs with associated HII regions than for GMCs without such associations seen in the LMC (Fukui et al. 1999; Blitz et al. 2005) seems to point in this direction. In addition, GMCs form in spiral shocks. As a result, the Lagrangian mass elements from which a cloud forms are probably subjected to a rising pressure as they enter the arm region, and then experience a falling pressure as the cloud moves out of the arm. This may have important effects on GMC evolution, and we explore the effects of more complex boundary conditions in Paper II. A related issue in GMC evolution, which we will also explore, is the effect of the apparent existence of column density thresholds for star formation. If clouds cannot begin forming stars until they accumulate a certain column of molecular mass, then feedback in GMCs will not start up until some time after the cloud first becomes molecular. This lag may affect GMC evolution.

There are also several limitations associated with our treatment of HII regions. We assume that the mass of the cloud is large enough that its evolution is dominated by HII regions, not protostellar outflows. We assume that the clouds are spherical, which means that all the energy injected by HII regions goes into internal motions, whereas in fact some of it goes into moving the entire cloud. Finally, we neglect possible energy injection by HII regions after merging. In our model, shells driven by small HII regions or those in very turbulent clouds may drop to expansion velocities below the cloud velocity dispersion well before the driving stars burn out. At this point the HII region will cease to drive a coherent expanding shell, and we approximate that the energy injection ceases. However, if the driving stars continue to ionize a part of the cloud, there is another potential driving mechanism. Clumps of gas that enter the ionized region will be photoevaporated on one side, and therefore will be rocketed away from the ionizing stars. Even though the resulting thrust is not enough to drive the clumps out of the HII region entirely, since the expansion velocity is smaller than the cloud velocity dispersion, it can still alter the trajectories of gas clumps and potentially inject energy (Tan 2001). This effect could be important in the cases where we find that HII regions cannot support GMCs because the velocity dispersion required to hold up the cloud is comparable to or larger than the ionized gas sound speed. Determining whether this effect is significant will require either more detailed theoretical treatment or numerical simulations. Despite these caveats, though, our results in § 6.3-6.4 and our analysis in § 7.1 show that our conclusions regarding the lifetime and evolutionary history of GMCs are quite robust against changes in the assumed efficiency with which HII regions drive turbulent motions or the rate at which those turbulent motions decay.

8. CONCLUSIONS

In this Paper we derive the basic equations governing the evolution of the mass, radius, and velocity dispersion of giant molecular clouds under the approximation of homologous motion. We construct simple models for the rate at which turbulent motions decay due to radiation from isothermal shocks and for the rate at which HII regions driven by massive stars within the cloud drive

turbulent motions, and we use these to study the global evolution and energetic balance of GMCs. This enables us to build GMC models in which we neither assume energetic and virial balance, nor neglect the effects of feedback. Thus, we are able for the first time to address critical questions such as whether GMCs are in virial or energetic equilibrium, how long they live, what determines their lifetimes and star formation histories, and what determines properties such as column density and virial parameter that appear to be roughly the same for all GMCs.

Our primary conclusion is that giant molecular clouds with observed properties are indeed quasi-equilibrium objects. The rate at which they lose energy via radiation from isothermal shocks is roughly balanced by the rate at which HII regions from star formation inject energy back into the cloud. This feedback keeps them virialized, $\alpha_{\text{vir}} = 1 - 2$, and keeps them at the observed column density $N_H \approx 1.5 \times 10^{22} \text{ cm}^{-2}$. Our results suggest that this column density, which appears to be generic for GMCs both in the Milky Way and in other galaxies where GMCs are observable, is in fact the result of feedback, since the efficiency of star formation feedback varies with column density, and the observed column density corresponds to the one required for equilibrium. Whether the GMC formation process, particularly the passage through an overdense and overpressured spiral shock, also plays a role in selecting the GMC column density is at this point an open question, one we will address in Paper II.

The duration of the equilibrium state of a GMC depends on cloud mass, but for clouds $\gtrsim 10^6 M_\odot$ in mass it lasts for 2 – 3 crossing times, or roughly 30 Myr. The dominant destruction mechanism for GMCs is dynamical unbinding by the momentum delivered by an expanding HII region, but for massive clouds this unbinding does not happen until HII regions have photoionized away $\sim 90\%$ of the GMC mass. Smaller clouds are dynamically disrupted by HII regions in ~ 10 Myr while $\sim 50\%$ of their mass is still in molecular form, but it is unclear if this disruption actually destroys their molecular material or simply breaks it into smaller, mutually unbound clouds.

Overall, our models produce a picture of GMCs that is quite different than that suggested by models in which GMCs are gravitationally unbound or in which feedback from star formation is neglected. Models that neglect feedback appear incapable of reproducing the observed lifetimes and properties of the GMC population. We conclude that any reasonable model of GMC evolution cannot neglect the effects of star formation feedback, and that even a simple model of feedback such as the one we use here produces good agreement with the observed properties of GMCs.

We thank E. C. Ostriker, J. P. Ostriker, E. Rosolowsky, J. M. Stone, and J. C. Tan for helpful discussions, and the anonymous referees for useful comments. Support for this work was provided by NASA through Hubble Fellowship grant #HSF-HF-01186 awarded by the Space Telescope Science Institute, which is operated by the Association of Universities for Research in Astronomy, Inc., for NASA, under contract NAS 5-26555 (MRK), by NSERC and the Canada Research Chairs Program

(CDM), and by the NSF through grants AST-0098365 and AST-0606831 (CFM).

APPENDIX

A. DERIVATION OF THE VIRIAL THEOREM FOR AN EVAPORATING CLOUD

Here we derive the equation of motion for an evaporating homologous cloud, which is a generalization of the Eulerian Virial Theorem (EVT, McKee & Zweibel 1992). Gas in the cloud is injected into the wind at a rate $\dot{\rho}$, so the continuity equation for the cloud is

$$\frac{\partial \rho}{\partial t} = -\nabla \cdot \rho \mathbf{v} + \dot{\rho}, \quad (\text{A1})$$

where ρ and \mathbf{v} are understood to be the density and velocity of cloud and not wind material. The wind satisfies its own continuity equation $\partial \rho_w / \partial t = -\nabla \cdot \rho_w \mathbf{v}_w - \dot{\rho}$, so that the summed equation $\partial(\rho + \rho_w) = -\nabla \cdot (\rho \mathbf{v} + \rho_w \mathbf{v}_w)$ is simply the ordinary continuity equation. The equation of momentum conservation for the cloud gas is

$$\frac{\partial}{\partial t}(\rho \mathbf{v}) = -\nabla \cdot (\mathbf{\Pi} - \mathbf{T}_M) + \rho \mathbf{g} + \dot{\rho}(\mathbf{v} + \mathbf{v}'_{\text{ej}}), \quad (\text{A2})$$

where $\mathbf{\Pi}$ is the gas pressure tensor, $\mathbf{T}_M \equiv [\mathbf{B}\mathbf{B} - (1/2)B^2\mathbf{I}]/(4\pi)$ is the Maxwell stress tensor, \mathbf{B} is the magnetic field, and \mathbf{g} is the gravitational force per unit mass. Intuitively, the $\dot{\rho}\mathbf{v}$ term represents the change in cloud momentum due to mass being transferred into the wind, and $\dot{\rho}\mathbf{v}'_{\text{ej}}$ is the recoil momentum from the ejection. As with the continuity equation, there is a corresponding momentum equation for the wind.

We now follow McKee & Zweibel (1992) in deriving the EVT for a cloud with a wind. The moment of inertia of the cloud is

$$I_{\text{cl}} \equiv \int_{V_{\text{vir}}} \rho r^2 dV, \quad (\text{A3})$$

where the fixed volume of integration V_{vir} is chosen to be sufficiently large that it includes the entire cloud at all times. Taking the time derivative

$$\begin{aligned} \dot{I}_{\text{cl}} &= - \int_{V_{\text{vir}}} (\nabla \cdot \rho \mathbf{v}) r^2 dV + \int_{V_{\text{vir}}} \dot{\rho} r^2 dV \\ &= - \int_{S_{\text{vir}}} (\rho \mathbf{v} r^2) \cdot d\mathbf{S} + 2 \int_{V_{\text{vir}}} \rho \mathbf{v} \cdot \mathbf{r} dV + a_{\text{I}} \dot{M}_{\text{cl}} R_{\text{cl}}^2 \end{aligned} \quad (\text{A4})$$

where S_{vir} is the surface of the volume V_{vir} , and

$$a_{\text{I}} \equiv \frac{3 - k_{\rho}}{5 - k_{\rho}}. \quad (\text{A5})$$

Differentiating again,

$$\begin{aligned} \frac{1}{2} \ddot{I}_{\text{cl}} &= -\frac{1}{2} \int_{S_{\text{vir}}} r^2 \frac{\partial}{\partial t} (\rho \mathbf{v}) \cdot d\mathbf{S} + \int_{V_{\text{vir}}} \frac{\partial}{\partial t} (\rho \mathbf{v}) \cdot \mathbf{r} dV \\ &\quad + \frac{1}{2} a_{\text{I}} \ddot{M}_{\text{cl}} R_{\text{cl}}^2 + a_{\text{I}} \dot{M}_{\text{cl}} R_{\text{cl}} \dot{R}_{\text{cl}}. \end{aligned} \quad (\text{A6})$$

The time derivative can be taken out of the integral in the first term because S_{vir} is fixed, and for the second term we can substitute for the integrand using the momentum equation (A2). This gives

$$\begin{aligned} \frac{1}{2} \ddot{I}_{\text{cl}} &= -\frac{1}{2} \frac{d}{dt} \int_{S_{\text{vir}}} r^2 \rho \mathbf{v} \cdot d\mathbf{S} - \int_{V_{\text{vir}}} \{ \mathbf{r} \cdot [\nabla \cdot (\mathbf{\Pi} - \mathbf{T}_M)] - \rho \mathbf{v} \cdot \mathbf{g} \} dV \\ &\quad + \int_{V_{\text{vir}}} \dot{\rho} \mathbf{r} \cdot \mathbf{v} dV + \int_{V_{\text{vir}}} \dot{\rho} r v'_{\text{ej}} dV + \frac{1}{2} a_{\text{I}} \ddot{M}_{\text{cl}} R_{\text{cl}}^2 + a_{\text{I}} \dot{M}_{\text{cl}} R_{\text{cl}} \dot{R}_{\text{cl}}. \end{aligned} \quad (\text{A7})$$

To evaluate the term $\int_{V_{\text{vir}}} \dot{\rho} \mathbf{r} \cdot \mathbf{v} dV$, we make use of our homology assumption, which allows us to write the velocity at any point in the cloud as

$$\mathbf{v} = \mathbf{r} \frac{\dot{R}_{\text{cl}}}{R_{\text{cl}}} + \mathbf{v}_{\text{turb}}, \quad (\text{A8})$$

where the first term represents homologous expansion or contraction of the cloud, and the second is a turbulent velocity that carries no net radial flux of matter. Thus, $\int_{V_{\text{vir}}} \rho \mathbf{r} \cdot \mathbf{v}_{\text{turb}} dV = 0$, and $\int_{V_{\text{vir}}} \dot{\rho} \mathbf{r} \cdot \mathbf{v} = \int_{V_{\text{vir}}} \dot{\rho} r^2 \dot{R}_{\text{cl}} / R_{\text{cl}}$.

This allows us to write the final EVT,

$$\begin{aligned} \frac{1}{2} \ddot{I}_{\text{cl}} &= 2(\mathcal{T} - \mathcal{T}_0) + \mathcal{B} + \mathcal{W} - \frac{1}{2} \frac{d}{dt} \int_{S_{\text{vir}}} (\rho \mathbf{v} r^2) \cdot d\mathbf{S} \\ &\quad + 2a_{\text{I}} \dot{M}_{\text{cl}} R_{\text{cl}} \dot{R}_{\text{cl}} + \frac{3 - k_{\rho}}{4 - k_{\rho}} \dot{M}_{\text{cl}} R_{\text{cl}} v'_{\text{ej}} + \frac{1}{2} a_{\text{I}} \ddot{M}_{\text{cl}} R_{\text{cl}}^2. \end{aligned} \quad (\text{A9})$$

In this equation, the kinetic term is

$$\mathcal{T} = \frac{1}{2} \int_{V_{\text{vir}}} (3P + \rho v^2) dV \quad (\text{A10})$$

for gas thermal pressure P , the surface term is

$$\mathcal{T}_0 = \frac{1}{2} \int_{S_{\text{vir}}} \mathbf{r} \cdot \mathbf{\Pi} \cdot d\mathbf{S}, \quad (\text{A11})$$

the gravitational term is

$$\mathcal{W} = \int_{V_{\text{vir}}} \rho \mathbf{r} \cdot \mathbf{g} dV, \quad (\text{A12})$$

and the magnetic term is

$$\mathcal{B} = \frac{1}{8\pi} \int_{V_{\text{vir}}} (B^2 - B_0^2) dV, \quad (\text{A13})$$

where B_0 is the background magnetic field far from the cloud, and we require that V_{vir} be large enough to include the full volume over which the background field is distorted by the presence of the cloud.

B. DERIVATION OF ENERGY CONSERVATION FOR AN EVAPORATING CLOUD

Here we derive the equation of energy conservation for an evaporating homologous cloud. First, we rewrite the momentum equation (A2) in a slightly different form,

$$\rho \frac{d\mathbf{v}}{dt} = -\nabla P - \rho \nabla \phi + \frac{\mathbf{J} \times \mathbf{B}}{c} + \dot{\rho} \mathbf{v}'_{\text{ej}}, \quad (\text{B1})$$

where the terms on the right hand side are the pressure, gravitational, and Lorentz forces, ϕ is the gravitational potential, \mathbf{J} is the current density, and we have replaced the pressure tensor $\mathbf{\Pi}$ with the isotropic pressure $P\mathbf{I}$ under the assumption that viscosity is negligible. Taking the dot product of (B1) with \mathbf{v} yields

$$\frac{\partial}{\partial t} \left(\frac{1}{2} \rho v^2 \right) + \nabla \cdot \left(\frac{1}{2} \rho \mathbf{v} v^2 \right) = -\mathbf{v} \cdot \nabla P - \rho \mathbf{v} \cdot \nabla \phi + \frac{\mathbf{v}}{c} \cdot (\mathbf{J} \times \mathbf{B}) + \dot{\rho} \left(\frac{1}{2} v^2 + \mathbf{v} \cdot \mathbf{v}'_{\text{ej}} \right). \quad (\text{B2})$$

Using the continuity equation, we can rewrite the gravitational work term as

$$-\rho \mathbf{v} \cdot \nabla \phi = -\nabla \cdot \rho \mathbf{v} \phi + \phi \nabla \cdot \rho \mathbf{v} \quad (\text{B3})$$

$$= -\nabla \cdot \rho \mathbf{v} \phi - \frac{\partial}{\partial t} (\rho \phi) + \rho \frac{\partial \phi}{\partial t} + \dot{\rho} \phi. \quad (\text{B4})$$

Similarly, we can rewrite the magnetic work term using Poynting's Theorem, which in the MHD approximation is

$$\frac{1}{8\pi} \frac{\partial}{\partial t} (B^2 - B_0^2) + \nabla \cdot \mathbf{S}_p = -\mathbf{J} \cdot \mathbf{E} = -\frac{\mathbf{v}}{c} \cdot (\mathbf{J} \times \mathbf{B}), \quad (\text{B5})$$

where \mathbf{S}_p is the Poynting flux, and we have used the fact that B_0 is constant to include it in the time derivative for future convenience. Substituting into (B2) gives the equation for the time-evolution of the non-thermal energy,

$$\frac{\partial}{\partial t} \left(\frac{1}{2} \rho v^2 + \rho \phi + \frac{B^2 - B_0^2}{8\pi} \right) + \nabla \cdot \rho \mathbf{v} \left(\frac{1}{2} v^2 + \phi \right) + \nabla \cdot \mathbf{S}_p = -\mathbf{v} \cdot \nabla P + \rho \frac{\partial \phi}{\partial t} + \dot{\rho} \left(\frac{1}{2} v^2 + \phi + \mathbf{v} \cdot \mathbf{v}'_{\text{ej}} \right). \quad (\text{B6})$$

To include the internal energy, we write down the first law of thermodynamics,

$$\rho \frac{de}{dt} + P \nabla \cdot \mathbf{v} = \Gamma - \Lambda, \quad (\text{B7})$$

where e is the internal energy per unit mass and Γ and Λ are the rates of radiative energy gain and loss per unit volume. Combining this with the continuity equation gives the evolution equation for the internal energy,

$$\frac{\partial}{\partial t} (\rho e) + \nabla \cdot \rho \mathbf{v} \left(e + \frac{P}{\rho} \right) = \dot{\rho} e + \mathbf{v} \cdot \nabla P + \Gamma - \Lambda. \quad (\text{B8})$$

Adding together the evolution equations (B6) and (B8) for the non-thermal and thermal energies gives the total energy equation

$$\begin{aligned} \frac{\partial}{\partial t} \left[\rho \left(\frac{1}{2} v^2 + e + \phi \right) + \frac{B^2 - B_0^2}{8\pi} \right] + \nabla \cdot \rho \mathbf{v} \left(\frac{1}{2} v^2 + e + \frac{P}{\rho} + \phi \right) + \nabla \cdot \mathbf{S}_p \\ = \rho \frac{\partial \phi}{\partial t} + \dot{\rho} \left(\frac{1}{2} v^2 + e + \phi + \mathbf{v} \cdot \mathbf{v}'_{\text{ej}} \right) + \Gamma - \Lambda. \end{aligned} \quad (\text{B9})$$

To derive the global form of the energy equation, we integrate over the virial volume V_{vir} , which gives

$$\begin{aligned} \frac{d\mathcal{E}}{dt} + \int_{S_{\text{vir}}} \left[\rho \left(\frac{1}{2}v^2 + e + \phi \right) + P \right] \mathbf{v} \cdot d\mathbf{S} + \int_{S_{\text{vir}}} \mathbf{S}_p \cdot d\mathbf{S} \\ = \frac{1}{2} \int_{V_{\text{vir}}} \rho \frac{\partial \phi}{\partial t} dV + \frac{\dot{M}_{\text{cl}}}{M_{\text{cl}}} (\mathcal{E} - \mathcal{B}) + \left(\frac{3 - k_\rho}{4 - k_\rho} \right) \dot{M}_{\text{cl}} \dot{R}_{\text{cl}} v'_{\text{ej}} + \mathcal{G}_{\text{cl}} - \mathcal{L}_{\text{cl}}, \end{aligned} \quad (\text{B10})$$

where

$$\mathcal{E} = \int_{V_{\text{cl}}} \left[\rho \left(\frac{1}{2}v^2 + e + \frac{1}{2}\phi \right) + \frac{B^2 - B_0^2}{8\pi} \right] dV \quad (\text{B11})$$

is the total energy in the cloud, \mathcal{G}_{cl} and \mathcal{L}_{cl} are the total rates of radiative energy gain and loss integrated over the cloud, and we have used our assumption of homologous motion to evaluate the terms involving $\dot{\rho}$ and \mathbf{v}'_{ej} . To evaluate the first integral on the left-hand side, we note all the terms proportional to density vanish at the cloud surface because the ambient material has zero density, but that constant pressure and zero density correspond to an incompressible fluid, so the velocity of the ambient medium across the virial surface is related to the velocity of the cloud surface by $v = \dot{R}_{\text{cl}}(R_{\text{cl}}^2/R_{\text{vir}}^2)$. This implies that

$$\int_{S_{\text{vir}}} \left[\rho \left(\frac{1}{2}v^2 + e + \phi \right) + P \right] \mathbf{v} \cdot d\mathbf{S} = 4\pi P_{\text{amb}} R_{\text{cl}}^2 \dot{R}_{\text{cl}}. \quad (\text{B12})$$

To evaluate the integral on the right-hand side, recall that gas in the wind contributes negligibly to the gravitational potential. Since the potential arises solely from cloud material, we can write (Shu 1992)

$$\frac{1}{2} \int_{V_{\text{vir}}} \rho \frac{\partial \phi}{\partial t} dV = \frac{1}{2} \int_{V_{\text{vir}}} \frac{\partial \rho}{\partial t} \phi dV = \left(\frac{\dot{M}_{\text{cl}}}{M_{\text{cl}}} \right) \frac{1}{2} \int_{V_{\text{vir}}} \rho \phi dV = \frac{\dot{M}_{\text{cl}}}{M_{\text{cl}}} \mathcal{W}. \quad (\text{B13})$$

Finally, we must evaluate $\int_{S_{\text{vir}}} \mathbf{S}_p \cdot d\mathbf{S}$, which represents the flux of magnetic energy across the virial surface as it is carried off by the wind. This is uncertain, because it depends on the process by which the mass is removed. As in § 2.1, we write the magnetic energy as a sum of turbulent and non-turbulent contributions, $1/(8\pi) \int_{V_{\text{vir}}} (B^2 - B_0^2) dV = \mathcal{B} = \mathcal{B}_{\text{non-turb}} + \mathcal{B}_{\text{turb}}$. For the turbulent part, we assume that the wind does not change the nature of the MHD turbulence within the cloud, so the turbulent magnetic energy remains proportional to the turbulent kinetic energy. Since the loss of turbulent energy accompanying mass loss is $\int_{V_{\text{vir}}} 3\dot{\rho}v^2/2 dV = (\dot{M}_{\text{cl}}/M_{\text{cl}})\mathcal{T}_{\text{turb}}$, this requires that the flux of turbulent magnetic energy be $\partial\mathcal{B}_{\text{turb}}/\partial t = (\dot{M}_{\text{cl}}/M_{\text{cl}})\mathcal{B}_{\text{turb}}$. For the non-turbulent part, for simplicity and based on the observation that GMCs have roughly constant mass-to-flux ratios (Crutcher 1999), we assume that the mass-to-flux ratio remains constant as the cloud loses mass. Since $\mathcal{B}_{\text{non-turb}} \propto \Phi^2$, this implies $\partial\mathcal{B}_{\text{non-turb}}/\partial t = 2(\dot{\Phi}/\Phi)\mathcal{B}_{\text{non-turb}} = 2(\dot{M}_{\text{cl}}/M_{\text{cl}})\mathcal{B}_{\text{non-turb}}$. Thus, we can write

$$\int_{S_{\text{vir}}} \mathbf{S}_p \cdot d\mathbf{S} = -\frac{\dot{M}_{\text{cl}}}{M_{\text{cl}}} (\mathcal{B}_{\text{turb}} + 2\mathcal{B}_{\text{non-turb}}) = -\frac{\dot{M}_{\text{cl}}}{M_{\text{cl}}} (\mathcal{B} - \eta_{\text{B}}^2 \mathcal{W}). \quad (\text{B14})$$

Substituting (B12), (B13), and (B14) into (B10), we arrive at the final energy equation for the cloud:

$$\frac{d\mathcal{E}}{dt} = \frac{\dot{M}_{\text{cl}}}{M_{\text{cl}}} [\mathcal{E} + (1 - \eta_{\text{B}}^2)\mathcal{W}] - 4\pi P_{\text{amb}} R_{\text{cl}}^2 \dot{R}_{\text{cl}} + \left(\frac{3 - k_\rho}{4 - k_\rho} \right) \dot{M}_{\text{cl}} \dot{R}_{\text{cl}} v'_{\text{ej}} + \mathcal{G}_{\text{cl}} - \mathcal{L}_{\text{cl}}. \quad (\text{B15})$$

REFERENCES

- Basu, S. & Murali, C. 2001, *ApJ*, 551, 743
 Bertoldi, F. & McKee, C. F. 1990, *ApJ*, 354, 529
 —. 1992, *ApJ*, 395, 140
 Blaauw, A. 1964, *ARA&A*, 2, 213
 Blitz, L., Fukui, Y., Kawamura, A., Leroy, A., Mizuno, N., & Rosolowsky, E. 2005, *Protostars and Planets V*, in press, astro-ph/0602600
 Blitz, L. & Shu, F. H. 1980, *ApJ*, 238, 148
 Bonnell, I. A., Dobbs, C. L., Robitaille, T. P., & Pringle, J. E. 2006, *MNRAS*, 365, 37
 Cho, J. & Lazarian, A. 2003, *MNRAS*, 345, 325
 Clark, P. C. & Bonnell, I. A. 2004, *MNRAS*, 347, L36
 Clark, P. C., Bonnell, I. A., Zinnecker, H., & Bate, M. R. 2005, *MNRAS*, 359, 809
 Crutcher, R. M. 1999, *ApJ*, 520, 706
 Dale, J. E., Bonnell, I. A., Clarke, C. J., & Bate, M. R. 2005, *MNRAS*, 358, 291
 Dobbs, C. L., Bonnell, I. A., & Pringle, J. E. 2006, *MNRAS*, submitted, astro-ph/0602103
 Elmegreen, B. G. 2000, *ApJ*, 530, 277
 Engargiola, G., Plambeck, R. L., Rosolowsky, E., & Blitz, L. 2003, *ApJS*, 149, 343
 Fukui, Y., Mizuno, N., Yamaguchi, R., Mizuno, A., Onishi, T., Ogawa, H., Yonekura, Y., Kawamura, A., Tachihara, K., Xiao, K., Yamaguchi, N., Hara, A., Hayakawa, T., Kato, S., Abe, R., Saito, H., Mano, S., Matsunaga, K., Mine, Y., Moriguchi, Y., Aoyama, H., Asayama, S.-i., Yoshikawa, N., & Rubio, M. 1999, *PASJ*, 51, 745
 Gao, Y. & Solomon, P. M. 2004, *ApJ*, 606, 271
 Hartmann, L., Ballesteros-Paredes, J., & Bergin, E. A. 2001, *ApJ*, 562, 852
 Hatchell, J., Richer, J. S., Fuller, G. A., Quattrough, C. J., Ladd, E. F., & Chandler, C. J. 2005, *A&A*, 440, 151
 Heyer, M. H. & Brunt, C. M. 2004, *ApJ*, 615, L45
 Heyer, M. H., Carpenter, J. M., & Snell, R. L. 2001, *ApJ*, 551, 852
 Huff, E. M. & Stahler, S. 2006, *ApJ*, in press, astro-ph/0603138
 Johnstone, D., Di Francesco, J., & Kirk, H. 2004, *ApJ*, 611, L45
 Kennicutt, R. C. 1998, *ARA&A*, 36, 189

- Kim, W. & Ostriker, E. C. 2001, *ApJ*, 559, 70
- Kim, W., Ostriker, E. C., & Stone, J. M. 2002, *ApJ*, 581, 1080
- , 2003, *ApJ*, 599, 1157
- Kornreich, P. & Scalo, J. 2000, *ApJ*, 531, 366
- Kroupa, P. 2001, *MNRAS*, 322, 231
- Kroupa, P. 2002, in *ASP Conf. Ser. 285: Modes of Star Formation and the Origin of Field Populations*, ed. E. K. Grebel & W. Brandner, 86+
- Krumholz, M. R. & McKee, C. F. 2005, *ApJ*, 630, 250
- Krumholz, M. R., McKee, C. F., & Klein, R. I. 2006a, *ApJ*, 638, 369
- Krumholz, M. R., Stone, J. M., & Gardiner, T. A. 2006b, *ApJ*, submitted, astro-ph/0606539
- Krumholz, M. R. & Tan, J. C. 2006, *ApJ*, submitted, astro-ph/0606277
- Lada, C. J. & Lada, E. A. 2003, *ARA&A*, 41, 57
- Larson, R. B. 1981, *MNRAS*, 194, 809
- Li, W., Evans, N. J., & Lada, E. A. 1997, *ApJ*, 488, 277
- Li, Z.-Y. & Nakamura, F. 2006, *ApJ*, 640, L187
- Luna, A., Bronfman, L., Carrasco, L., & May, J. 2006, *ApJ*, in press, astro-ph/0512046
- Mac Low, M. 1999, *ApJ*, 524, 169
- Mac Low, M. & Klessen, R. S. 2004, *Reviews of Modern Physics*, 76, 125
- Mac Low, M., Klessen, R. S., Burkert, A., & Smith, M. D. 1998, *Physical Review Letters*, 80, 2754
- Mac Low, M.-M., Toraskar, J., Oishi, J. S., & Abel, T. 2006, *ApJ*, submitted, astro-ph/0605501
- Matzner, C. D. 1999, PhD thesis, University of California, Berkeley
- , 2002, *ApJ*, 566, 302
- Matzner, C. D. & McKee, C. F. 1999, in *Star Formation 1999, Proceedings of Star Formation 1999, held in Nagoya, Japan, June 21 - 25, 1999*, Editor: T. Nakamoto, Nobeyama Radio Observatory, p. 353-357, ed. T. Nakamoto, 353-357
- Matzner, C. D. & McKee, C. F. 2000, *ApJ*, 545, 364
- McKee, C. F. 1989, *ApJ*, 345, 782
- McKee, C. F. & Tan, J. C. 2003, *ApJ*, 585, 850
- McKee, C. F., van Buren, D., & Lazareff, B. 1984, *ApJ*, 278, L115
- McKee, C. F. & Williams, J. P. 1997, *ApJ*, 476, 144
- McKee, C. F. & Zweibel, E. G. 1992, *ApJ*, 399, 551
- McKee, C. F., Zweibel, E. G., Goodman, A. A., & Heiles, C. 1993, in *Protostars and Planets III*, 327
- Mellema, G., Arthur, S. J., Henney, W. J., Iliev, I. T., & Shapiro, P. R. 2005, *ApJ*, submitted, astro-ph/0512554
- Mouschovias, T. C. & Spitzer, L. 1976, *ApJ*, 210, 326
- Nakamura, F., McKee, C. F., Klein, R. I., & Fisher, R. T. 2006, *ApJ*, submitted
- Onishi, T., Kawamura, A., Abe, R., Yamaguchi, N., Saito, H., Moriguchi, Y., Mizuno, A., Ogawa, H., & Fukui, Y. 1999, *PASJ*, 51, 871
- Onishi, T., Mizuno, A., Kawamura, A., Ogawa, H., & Fukui, Y. 1998, *ApJ*, 502, 296
- Onishi, T., Mizuno, A., Kawamura, A., Tachihara, K., & Fukui, Y. 2002, *ApJ*, 575, 950
- Ossenkopf, V. & Mac Low, M.-M. 2002, *A&A*, 390, 307
- Padoan, P. & Nordlund, Å. 1999, *ApJ*, 526, 279
- Parravano, A., Hollenbach, D. J., & McKee, C. F. 2003, *ApJ*, 584, 797
- Quillen, A. C., Thorndike, S. L., Cunningham, A., Frank, A., Gutermuth, R. A., Blackman, E. G., Pipher, J. L., & Ridge, N. 2005, *ApJ*, 632, 941
- Richer, J. S., Shepherd, D. S., Cabrit, S., Bachiller, R., & Churchwell, E. 2000, *Protostars and Planets IV*, 867
- Rosolowsky, E. & Blitz, L. 2005, *ApJ*, 623, 826
- Rosolowsky, E., Engargiola, G., Plambeck, R., & Blitz, L. 2003, *ApJ*, 599, 258
- Rownd, B. K. & Young, J. S. 1999, *AJ*, 118, 670
- Shu, F. H. 1992, *Physics of Astrophysics, Vol. II* (University Science Books)
- Shu, F. H., Adams, F. C., & Lizano, S. 1987, *ARA&A*, 25, 23
- Slyz, A. D., Devriendt, J. E. G., Bryan, G., & Silk, J. 2005, *MNRAS*, 356, 737
- Solomon, P. M., Rivolo, A. R., Barrett, J., & Yahil, A. 1987, *ApJ*, 319, 730
- Stone, J. M., Ostriker, E. C., & Gammie, C. F. 1998, *ApJ*, 508, L99
- Sugimoto, K., Hanawa, T., & Fukuda, N. 2004, *ApJ*, 609, 810
- Tan, J. C. 2000, *ApJ*, 536, 173
- , 2001, PhD thesis, University of California, Berkeley
- Tan, J. C., Krumholz, M. R., & McKee, C. F. 2006, *ApJ*, 641, L121
- Tasker, E. J. & Bryan, G. L. 2006, *ApJ*, in press, astro-ph/0512027
- Tenorio-Tagle, G., Bodenheimer, P., & Yorke, H. W. 1985, *A&A*, 145, 70
- Vázquez-Semadeni, E., Ballesteros-Paredes, J., & Klessen, R. S. 2003, *ApJ*, 585, L131
- van Dishoeck, E. F. & Black, J. H. 1988, *ApJ*, 334, 771
- Vázquez-Semadeni, E., Ballesteros-Paredes, J., & Rodriguez, L. F. 1997, *ApJ*, 474, 292
- Vázquez-Semadeni, E., Ryu, D., Passot, T., Gonzalez, R. F., & Gazol, A. 2006, *ApJ*, submitted, astro-ph/0509127
- Whitworth, A. 1979, *MNRAS*, 186, 59
- Williams, J. P. & McKee, C. F. 1997, *ApJ*, 476, 166
- Wong, T. & Blitz, L. 2002, *ApJ*, 569, 157
- Wu, J., Evans, N. J., Gao, Y., Solomon, P. M., Shirley, Y. L., & Vanden Bout, P. A. 2005, *ApJ*, 635, L173
- Yorke, H. W., Tenorio-Tagle, G., Bodenheimer, P., & Rozyczka, M. 1989, *A&A*, 216, 207
- Zinnecker, H., McCaughrean, M. J., & Wilking, B. A. 1993, in *Protostars and Planets III*, 429-495
- Zuckerman, B. & Evans, N. J. 1974, *ApJ*, 192, L149